Arab American University

Faculty of Graduate Studies

Effects of Yb, Mn and Au transparent metal substrates on the structural and optical properties of phthalocyanine (ZnPC) thin films

By
Hadeel Mahmoud Zyoud

Supervisor
Prof. Dr. A.F.Qasrawi

This thesis was submitted in partial fulfillment of the requirements for the Master's degree in Physics

September/2019

Effects of Yb, Mn and Au transparent metal substrates on the structural and optical properties of phthalocyanine (ZnPC) thin films

By
Hadeel Mahmoud Zyoud

This thesis was defended successfully on 28/9/2019 and approved by:

Committee members — Signature

1. Prof. Atef Fayez Qasrawi (Supervisor) .....
2. Assoc. Prof. Ahmad Yousef Omar (Internal examiner) .....
3. Assoc. Prof. Mohammed Suleiman Shtaya (External examiner) .....

Declaration

The work in this thesis, unless otherwise referenced, is the researcher's own work and has not been submitted elsewhere for any other degree or qualification.

Student's Name: Hadeel Mahmoud Mostafa Zyoud

Acknowledgment

In the name of the God the most merciful the most beneficent who gave us a strength and knowledge to complete this work. This has proved to be a good experience. My deepest gratitude to my parents who gave me the encouragement in my educational trend, a special thanks for my genius supervisor Prof. Dr.Atef Qasrwai the one who deserve all my efforts, the one who was helpful and guidance for me during all my study period. This work could not have been completed without him. Special thanks for Mrs Olfat Omareya who submitted her help during the period I had worked in the laboratory. Iam so grateful to my best friends who shared their support in one way or another. I want to thank everyone who supported me to finalize this thesis and thanks go to my university.

Abstract

In this thesis, we attempted to alter the structural, optical and dielectric properties of ZnPC thin films through establishing a transparent metal surface that interacts with the organic material pthalocyanine (ZnPC) to form Plasmon-electron interacting media. For this purpose, the ZnPC thin films are coated onto glass, Yb, Au and Mn substrates of 150 nm thicknesses. The films are structurally, morphologically and optically analyzed. It was observed that while the Mn and Au substrates forces amorphous nature of growth of ZnPC films, the glass and Yb caused the growth of monoclinic phase of pthalocyanine. The Yb substrate increased the crystallite size and decreased the micro strain, dislocation density and stacking faults. Optically, ZnPC films exhibit strong absorption bands in the high and low energy range of spectrum. It is observed that while Mn substrate motivated the formation of wide band tails, Au and Yb formed narrower band tails. One result that is worthy of consideration is that the Mn substrate successfully increased the light absorbability by 21 times compared to Au and Yb substrates which increased the light absorbability by five and three times near 2.5 eV, respectively. Estimations of the effects of the metal substrates on the energy band gap have shown that these metals don't strongly affect the energy band gap. On the other hand, while the dielectric response at high frequency is not affected by the presence of metals, the dielectric spectra in the infrared range is enhanced by 37.3%, 57.5% and 181.95% when ZnPC was coated onto Yb, Mn and Au substrates, respectively, near 1.10 eV. The modeling of the imaginary part of the dielectric spectra assuming the validity of Drude -Lorentz model has shown that the metal substrates improves the drift mobility from 0.46 to 7.49, 6.86 and 7.50 cm^2/Vs when films were coated onto Yb, Au and Mn. While the Yb substrates decreased

the Plasmon frequency, the Au and Mn substrates highly increased it to levels that make it more appropriate for optoelectronic technology applications.

Keyword: electron-Plasmon frequency, absorbability, drift mobility, Yb, Mn, dielectric, X-ray.

List of contents

List of tables

List of figures

List of abbreviations

Abbreviations	Word
MPC	Metal Phalocyanine
PVD	Physical vapor deposition
ZnPC	Zinc Phalocyanine
Mn	Manganese
Yb	Ytterbium
Au	Gold
Eg	Energy band gap
XRD	X-Ray diffraction
M*	Mass effective
DOS	Density of states
α	Absorption coefficient
SEM	Scanning electron microscope
SF%	Stacking faults
IR	Infrared region
Rα	Absorbability
W_{pe}	Electron-Plasmon frequency
λ	Wavelength
κ	Propagation number
K	Extinction coefficient
T	Transmission

R	Reflectance
N	Complex refractive index
ω	Angular frequency
δ	Dislocation density
ε	Strain

Chapter One
Introduction and literature survey

Nowadays, organic materials attracted the attention owing to the smart properties that they reveal. For example, metal pthalocynine (MPC) compounds ($C_{32}H_{16}N_8M$) captures the focus due to their thermal stability and high molecular symmetry [1]. They are sources of forming many compounds based on the metal that they are composed of such as: Mn, Co, Pt, Pb, Cu, Fe, Ni and Zn [2-5]. MPC were reported to be used in the fabrication of light emitting diodes (LED), field effect transistors, photovoltaic, memory, solar cells and sensors devices [6-10]. Zinc pthalocyanine (ZnPC) is one of the most important organic materials. Copper pthalocyanine (CuPC) were mentioned to have a large performance as memory devices. By introducing CuPC thin films between gold (Au) and indium tin oxide (ITO) layers they produced a high current on/off ratio of 10^6 and high current stability that indicated the possibility of using it as memory devices [8]. However, the reason beyond mentioning the CuPC films as an example, is that CuPC can be regarded as the closet to ZnPC due to the similar structures that both metals have. The atomic number of Cu and Zn are 30 and 29 respectively [1], so that ZnPC can have the same results that CuPC revealed. Moreover, ZnPC is widely used in solar cell applications due to the easy synthesizing and non-toxic properties [11]. Previous investigations of sandwiching ZnPC between Au and Aluminum (Al) layers have shown an enhancement in dielectric performance. In that study a large range of temperature and frequency measurements in the range of 93-470 K, and 0.1-20 kHz, respectively, were included. It was reported that the temperature and frequency affected the response of the dielectric constant greatly. Enhancing the dielectric constant

value make ZnPC suitable for fabrication of organic solar cells [12]. Furthermore, the high absorption coefficient that ZnPC displayed makes it preferable for photovoltaic applications [11], It was also mentioned that ZnPC exhibit an absorption coefficient values larger than that of ZnSe [13]. A thin layer of ZnPC between (ITO) and lead pthalocyanine (PbPC) has shown an improvement in the light absorbability also and in the hole carrier at the ITO electrode. It leaded to an increase in the power conversion efficiency (PCE) to 1.95 % [14]. Other works that concern with ZnPC photovoltaic properties used ZnPC:C_{60} onto ITO substrates. This deposition has shown an enhancement in the PCE and makes it reach 3.9 % [15].

MPC thin films were reported to be polymorphic [16], and exhibited α, β and γ phases. The α- phase represents a monoclinic structure and β could be orthorhombic, tetragonal, or monoclinic at room temperature. γ-phase is still remain to be not well understood [17]. A transformation from α → β phase [17] can occur by annealing process or a suitable substrate temperature. An investigation on ZnPC to study the phase transformation for both annealing and substrate temperature were carried out [18, 19]. ZnPC films have two absorption bands named Q and B-bands. Which result from $\pi \rightarrow \pi^*$ transitions [20]. ZnPC also were found to show direct and allowed transitions with energy band gap value of 1.97 eV [11]. Moreover, an important feature of ZnPC films has shown that the microcrystalline films of ZnPC provide longer diffusion for the exciton formation than nanocrystalline films [13]. On the other hand, ZnPC is reported to be defective material. The dislocation density exhibited values of 1.03×10^{14} line/cm^2 for film of thicknesses of 750 nm [6].

Various methods were used to produce ZnPC films such as organic molecular beam deposition (OMBD) [21], STM [22] and physical vapor deposition (PVD) [17]. ZnPC which were prepared by OMBD were coated onto silicon substrates [21]. Other works prepared ZnPC by STM technique. The films were kept at room temperature in ultra-high vacuum (UHV) using STM (JEOL-JAFM-4500XT) equipped with a preparation chamber [22]. In addition, the physical vapor deposition technique was widely used for preparation of ZnPC. For example, it was reported that cleaned glass was used to evaporate ZnPC by thermal evaporation technique under a vacuum of 10^{-6} mbar at room temperature [17].

Based on the above features, here in this work we target the deposition of ZnPC films onto transparent metal substrates ytterbium (Yb), gold (Au) and manganese (Mn) using the thermal evaporation technique under vacuum pressure of 10^{-5}mbar. The produced films are subjected to X-Ray diffraction to investigate the structural properties. In addition, the ultraviolet-visible light spectroscopy will be used to analyze the optical and dielectric performance of these Yb, Ay and Mn/semiconductors interfaces. Moreover, some computer simulations will be carried out to explore the optical conductivity parameters of the structure. Fortunately, no literature data were observed about Mn and Yb/ZnPC interfaces, and we aim to enrich the literature about them.

This thesis will include five chapters, chapter one will be an introduction about the current work. Chapter two is a theoretical background of our calculations and basic mathematics we employ to analyze the results. Chapter three is the experimental details of how these thin films and interfaces are designed and characterized. Chapter four shows the achieved results and discusses the observations. It reports the properties that we reveal and the

advantages we discovered in the films and chapter five is the conclusion of the work followed by the references.

Chapter Two
Theoretical background

2.1 X-ray diffraction

X-ray is an electromagnetic wave similar to the visible light with shorter wavelength [23]. X-ray diffraction is a technique used to discover the crystal structure. The diffraction of a monochromatic plane wave from a matter can be produced by scattering of the individual atoms to the incident waves and the interference of theses scattered waves [24].

2.2 Bragg's law:

The crystal structure is studied by the diffraction of high energy photons, neutrons and electrons. Diffracted beams may be found in a direction quite different than the incident direction. Thus, Bragg's law is a simple explanation of the diffracted beams from a crystal. It is supposed that the incident waves are reflected specularly (the incident beam angle equal to the reflected angle) from a parallel plane of atoms in the crystal. When the interference between reflected beams is constructive then diffraction can occur. Fig (2.1) represents planes of atoms in a crystal being separated by distance (d). The derivation of Bragg's law can be understood by considering the path difference equal to $2d\sin\theta = n\lambda$, where n is integer greater or equal 1.0. λ is the X-ray wavelength that equals to 1.5041 A° for Cu source [25], and θ is the angle that is measured from the plane, and d is the interplaner distance.

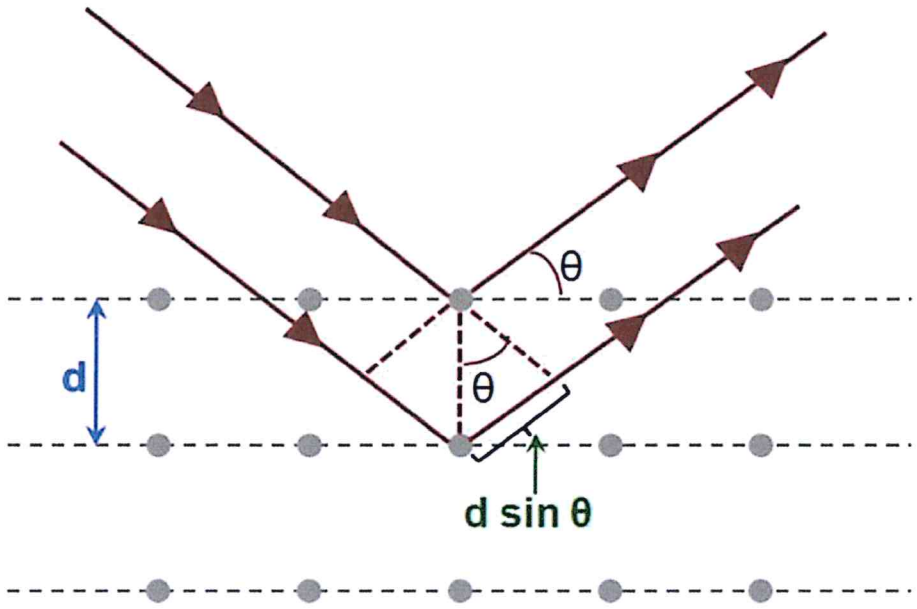

Fig (2.1): Conditions for Bragg law [25].

2.3 Crystal structures

Crystal structure is a manner in which atoms are arranged in a unit cell, where the unit cell is defined as the smallest repeating unit with full symmetry of the crystal structure [26], the cell is defined by three lattice constants (a, b, c) and the angles between them are (α, β, γ). Table (2.1) represent the famous 3-D crystal structures.

Table (2.1): 3-D crystal structures [26].

Structure type	Lattice constant	Angles
Cubic	$a_1 = a_2 = a_3$	$\alpha = \beta = \gamma = 90^o$
Tetragonal	$a_1 = a_2 \neq a_3$	$\alpha = \beta = \gamma = 90^o$
Orthorhombic	$A_1 \neq a_2 \neq a_3$	$\alpha = \beta = \gamma = 90^o$
Triagonal	$a_1 = a_2 = a_3$	$\alpha = \beta = \gamma < 120^o, \neq 90^o$
Hexagonal	$a_1 = a_2 \neq a_3$	$\alpha = \beta, \gamma = 120^o$
Monoclinic	$a_1 \neq a_2 \neq a_3$	$\alpha = \gamma = 90^o \neq \beta$
Triclinic	$a_1 \neq a_2 \neq a_3$	$\alpha \neq \beta \neq \gamma$

2.4 Derivation of Scherrer's equation

Scherrer expression is used for calculating the broadening in grain size [27]. Consider that Bragg's law for n=1 is multiplied by an integer m for both side of the equation then,

$$m\lambda = 2md\sin\theta \qquad \textbf{(2. 1)}$$

Now, consider the total thickness is $t = md$, equation (2.1) becomes,

$$m\lambda = 2t\sin\theta \qquad \textbf{(2. 2)}$$

The easier way to get Scherrer equation is the derivative of equation with respect to θ and t, remembering that $m\lambda$ is constant,

$$0 = 2\Delta t\sin\theta + 2t\cos\theta\Delta\theta \qquad \textbf{(2.3)}$$

$\Delta\theta$ Could be negative or positive, the absolute value must be taken and it reflects the peak full-width at half-height (FWHM) or the broadening of the peak, so recalling that Δt is d (interplaner distance), equation (2.3) becomes,

$$t = \frac{d \sin\theta}{\cos\theta \Delta\theta} \qquad \textbf{(2. 4)}$$

According to Bragg's law $d \sin\theta = \frac{\lambda}{2}$ for n=1, substituting this in equation (2.4)

$$t = \frac{\lambda}{2\cos\theta \Delta\theta} \qquad \textbf{(2. 5)}$$

Considering that $\beta = 2\Delta\theta$, β is the full width at half maximum (FWHM), then equation (2.5) is

$$t = \frac{\lambda}{\beta \cos\theta} \qquad \textbf{(2.6)}$$

If a Gaussian function (rather than a triangle function) is used to describe the peak a prefactor of 0.94 occurs so the Scherrer equation is given by

$$t = \frac{0.94\lambda}{\beta \cos\theta}, \qquad \textbf{(2.7)}$$

Where θ is the Bragg's angle.

2.5 structural parameters

The structural parameters include the grain size, strain, dislocation density and stacking faults and their equation formula are taken from previously published equations [28, 29], these parameters affects the mechanical properties of the crystal [30].

2.5.1 Grain size

The grain size is the diameter of individual grain in (nm), and it can be determined by Scherrer equation which was described in the previous section [31].

$$D = \frac{0.94\lambda}{\beta \cos\theta} \qquad \textbf{(2.9)}$$

Where β: is the broadening of the peak (FWHM) and θ : is the Bragg's angle in rad.

2.5.2 Strain

Strain is a deformation that results from a stress [30], and it is defined by the relation,

$$\varepsilon = \frac{\beta}{4\tan\theta} \qquad \textbf{(2.10)}$$

2.5.3 Dislocation density

Dislocation density is a type of defects that measures the number of dislocations in a unit area of crystalline material (lines/cm^2) [32]. It can be calculated from the equation.

$$\delta = \frac{15\varepsilon}{aD} \qquad (2.11)$$

a: is the crystal lattice constant, D: is the grain size and ε is the strain.

2.5.4 Stacking faults

Stacking faults are planar defects that describes the disorder in the crystallographic planes [33].

$$SF\% = \frac{2\pi^2\beta}{45\sqrt{3}\tan\theta} \qquad (2.12)$$

2.6 Optical properties of semiconductors

Optical properties of solid material can be classified as transmittance, reflectance and absorbance processes. These processes clearly appear in Fig (2.2). When the light incident on an optical medium, some of the light is reflected and some of it is transmitted and the remaining part is absorbed by the material atoms [34].

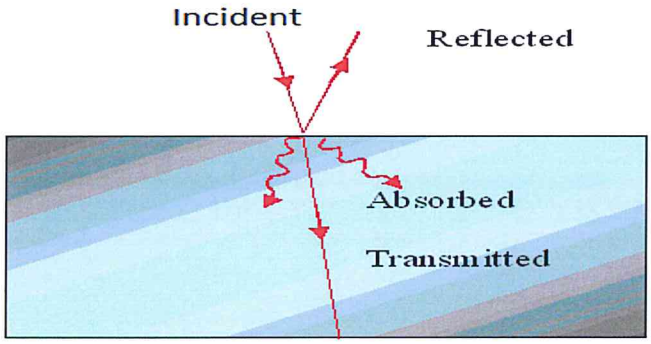

Fig (2.2): Reflection, transmission and absorption of a light incident on an optical material [34].

2.6.1 Absorption coefficient (α)

Absorption occurs when the electrons of the atom make transition from a lower occupied state to an empty upper state [34], the amount of light that is absorbed in the medium within a given thickness is called absorption coefficient [34], the absorption coefficient can be written based on Beer's law which state that,

$$I(z) = I_o e^{-\alpha z} \quad \textbf{(2.13)}$$

Where z is the material thickness, I_o is the optical intensity at z=0 and α is the absorption coefficient, where α is frequency dependent. This is the reason beyond that material sometimes absorbed one color but not the other [34]. The transmissivity of the light in the medium can be written according to the published equation [34],

$$T = (1 - R_1)(1 - R_2)e^{-\alpha z} \quad \textbf{(2.14)}$$

R_1 and R_2 is the reflectivities of the front and back layers of the medium and the term ($e^{-\alpha z}$) is the exponential decreased in the intensity that results from the absorption according to Beer's law.

If R_1 and R_2 are equal, equation (2.14) becomes,

$$T = (1 - R)^2 e^{-\alpha z} \quad \textbf{(2.15)}$$

If z=d, where d is the film thickness, then α becomes,

$$\alpha = \frac{-1}{d} \ln\left(\frac{T}{(1-R)^2}\right) \quad \textbf{(2.16)}$$

2.6.2 Electronic band structure

Atoms in solid material are close to each other, thus the outer orbital of the atoms are overlapping and interacts very strongly with each other. This interaction converts discrete levels of the atoms into bands. The electronic states within these bands are delocalized and processes the translational symmetry in the crystal [34].

2.6.3 Energy band gap

Energy band gap is a region where the electron can't be occupied in it. It is also called "forbidden region" [35]. Fig (2.3) shows the band structure of solids. The band gap is classified into two basic types, the direct and indirect band gap. If the angular momentum of electron and hole is the same at the maximum of the valence band and minimum of the conduction band the band gap called "direct band gap". The indirect band gap electron must pass through an intermediate process and transfer the momentum to the crystal lattice [34].

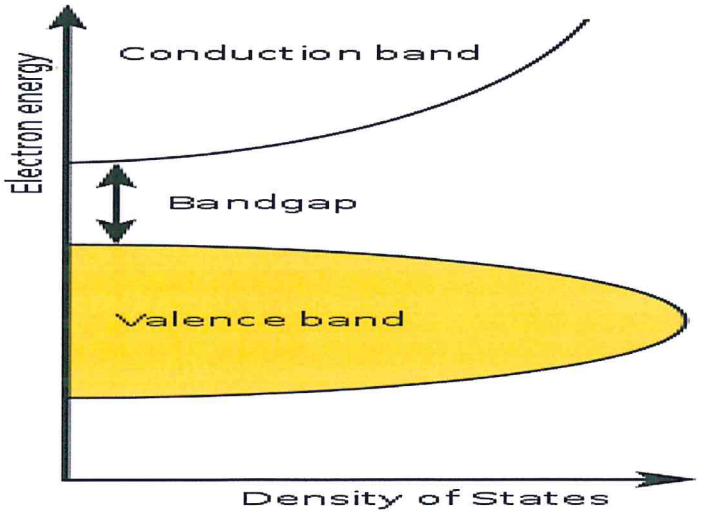

Fig (2.3): Electronic band structure of solids [35].

2.6.4 Tauc's equation

The absorption coefficient is very important to determine the energy band gap of semiconductors. Tauc's equation can be applied which is states that $(\alpha E) \propto (E - E_g)^p$ [34], Where α is the absorption coefficient, E is the photon energy and E_g is the energy band gap, p can take the values $\frac{1}{2}, \frac{3}{2}$, 2, 3, related to the direct allowed, direct forbidden, indirect allowed transition and indirect forbidden transitions, respectively.

2.6.5 Band tails

In disordered semiconductors there is an exponential distribution of states in the band gap called band tails. Band tails decreases exponentially as you move toward the middle of the band gap. It may exist near the conduction band or the valence band [36, 37]. Fig (2. 4) represents the distribution of these band tails in the band gap, the structural disordering could result from structure defects like vacancies, dislocation...) or by external defect like impurities [38]. The shape and size of theses tails depend on different types of disordering [39]. To determine the effect of these exponential distributions on the absorption coefficient, suppose a p-type degenerate material [40] and the perturbed part of valence band lies above the Fermi level, so the density of initial state is proportional to $|E_v|^{1/2}$, where E_v is the energy state with respect to the edge valence band. The final state density form band tail to the conduction band as appears in the equation

$$N_f = N_i e^{\frac{E}{E_o}} \qquad \textbf{(2.17)}$$

Where E_o is a parameter that describes the distribution of states but not their energy and it has a dimension of the energy. The absorption coefficient is proportional to the product of the final and initial state integrated all over the possible transition as appear in the following equation,

$$\alpha(h\nu) = A \int_{\xi_o}^{h\nu-\xi_o} |E_v|^{1/2} e^{\frac{E}{E_o}} dE \qquad \textbf{(2.18)}$$

Where A is constant and ξ_o is the energy state that measured with respect to the valence band.

In order to solve this integral, make a change of variable, let

$$x = \frac{h\nu - E}{E_o} \qquad \textbf{(2.19)}$$

and if x is substituted in the integral we get,

$$\alpha(h\nu) = -Ae^{\frac{h\nu}{E_o}} (E_o)^{3/2} \int_{\frac{h\nu+\xi_o}{E_o}}^{\frac{\xi_o}{E_o}} x^{1/2} e^{-x} dx \qquad \textbf{(2.20)}$$

The lower limit of the integral can be set to be 0 that because h is <<< E_o, then the solution of this integral can be written as

$$\alpha(h\nu) = A(E_o)^{3/2} e^{\frac{h\nu}{E_o}} \left[\frac{1}{2}(\pi)^{1/2} - \int_0^{\frac{\xi_o}{E_o}} x^{1/2} e^{-x} dx \right] \qquad \textbf{(2.21)}$$

The slope of the absorption on the semi logarithmic plot gives

$$\left[\frac{d\ln\alpha}{d(h\nu)}\right]^{-1} = E_o \tag{2.22}$$

$$\text{So, } \frac{1}{E_o} = \frac{d\ln\alpha}{d(h\nu)} \tag{2.23}$$

Finally the equation becomes

$$\alpha = \alpha_o e^{\frac{E}{E_o}}, \tag{2.24}$$

This equation represents the relation between the absorption coefficient and band tails.

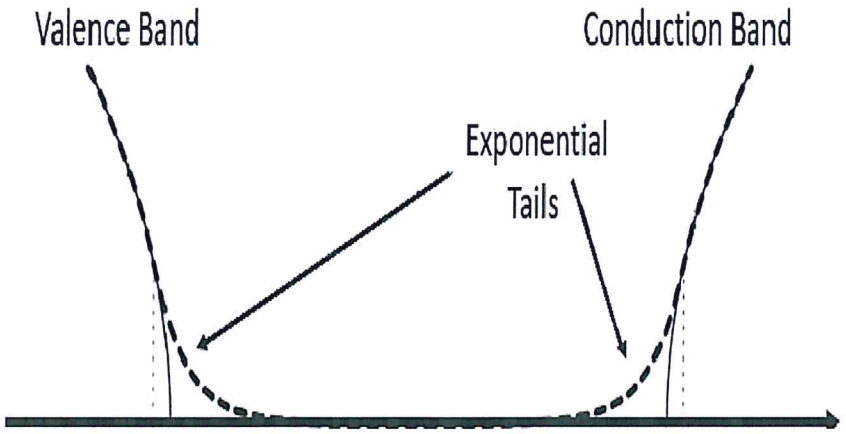

Fig (2.4): Band tails distribution among the band gap [40].

2.7 Dielectric constant

In order to obtain the dielectric constant formula, complex refractive index have to be introduced, where the refractive index is reported to be [41, 42],

$$\widetilde{N}_{complex} = \sqrt{\mu\varepsilon} \tag{2.25}$$

Where $\widetilde{N}_{complex}$ the complex refractive index and μ is is the magnetic permeability. Refractive index can be written in terms of its imaginary and real part,

$$\widehat{N}_{complex} = n + iK \tag{2.26}$$

Where

$$\widetilde{\mathrm{K}} = \frac{\omega}{C}\widetilde{N}_{complex} \tag{2.27}$$

Equation (2.27) can be derived from Maxwell's equations [41],

n is the refractive index and K is the extinction coefficient, K is vanishing for lossless material.

Now consider a non-magnetic material so that μ=1, then equation (2.25) becomes

$$\widehat{N}_{complex} = \sqrt{\varepsilon_{eff}} \tag{2.28}$$

With help of dielectric constant formula which states that,

$$\varepsilon_{eff} = \varepsilon_1 + i\varepsilon_2 \tag{2.29}$$

Substituting eq. (2.26) in eq. (2.28) we get,

$$\widetilde{N}^2{}_{complex} = \varepsilon_{eff} = (n + iK)^2 \tag{2.30}$$

Which yields,

$$\varepsilon_{eff} = n^2 - K^2 + i2nK \tag{2.31}$$

By comparing equation (2.31) with (2.29), it yields that the real and imaginary part of the dielectric constant are

$$\varepsilon_1 = n^2 - K^2 \tag{2.32}$$

$$\varepsilon_2 = 2nK \tag{2.33}$$

To find the relation between K and α consider that an electromagnetic wave propagates in a medium in the z-direction with an electric field of

$$\hat{E}(z,t) = E_o e^{i(kz-\omega t)} \tag{2.34}$$

Where κ is the wave number and ω is the angular frequency, the extinction coefficient K is related to λ and n by,

$$k = \frac{2\pi}{\lambda / \tilde{N}} = \frac{\omega \tilde{N}}{c} \tag{2.35}$$

Remembering that N is complex so we can express k in terms of $N_{complex}$, then substituting eq. (2.26) in (2.27) and (2.34),

$$k = \frac{\omega}{c}(n + iK) \tag{2.36}$$

$$\hat{E}(z,t) = E_o e^{i(\frac{\omega n z}{c} - \omega t)} e^{\frac{-Kz\omega}{c}} \tag{2.37}$$

We know that the optical intensity of light wave is proportional to the square of the electric field where I $\propto$ EE*, so that

$$I \propto e^{\frac{-2k\omega z}{c}} \tag{2.38}$$

If equation (2.38) is compared with Beer' equation (2.13) we can find that

$$2\frac{K\omega}{c} = \alpha = \frac{4\pi K}{\lambda} \tag{2.39}$$

The relation between the normal incident reflectivity and the dielectric constant is very useful in optical calculations [41], regarding a wave that propagates in a solid as appear in Fig (2.5)

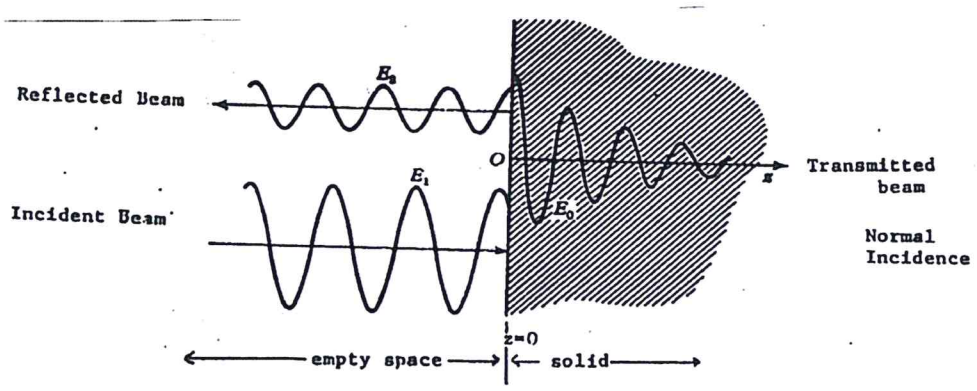

Fig (2.5): Schematic diagram for normal incident reflectivity [41].

$$\vec{E}_x = E_o e^{i(kz-\omega t)} \tag{2.40}$$

On the other hand, electric fields on the x-axis include both of the reflected and incident waves as appear in figure (2.5), where the propagation constant is $k = \frac{\omega}{c}\tilde{N}_{complex}$, so the electric field becomes

$$\vec{E} = \vec{E}_1 + \vec{E}_2 \tag{2.42}$$

Using Maxwell's equation which state that,

$$\nabla \times \vec{E} = -\frac{\mu}{c}\frac{\partial \vec{H}}{\partial t} = \frac{i\omega\mu}{c}\hat{H} \tag{2.43}$$

This yields,

$$\frac{\partial \vec{E}_x}{\partial z} = \frac{i\omega\mu}{c}\vec{H} \tag{2.44}$$

By deriving equation (2.41) and (2.40), and substituting it in equation (2.44) we can get

$$E_o k = E_1 \frac{\omega}{c} - E_2 \frac{\omega}{c} = E_o \frac{\omega}{c} \tilde{N}_{complex} \tag{2.45}$$

Which results in

$$E_1 - E_2 = E_o \tilde{N}_{complex} \tag{2.46}$$

Now combining equation (2.46) with that (2.42) and solving the two equations we can get,

$$E_2 = \frac{1}{2} E_o (1 - \tilde{N}_{complex}) \tag{2.47}$$

$$E_1 = \frac{1}{2} E_o (1 + \tilde{N}_{complex}) \tag{2.48}$$

With help of the fact that normal incident reflectivity is given by the relation,

$$R = \left| \frac{E_2}{E_1} \right|^2 \tag{2.49}$$

We can substitute (2.47) and (2.48) in (2.49), so R becomes,

$$R = \left| \frac{(1 - \tilde{N}_{complex})}{(1 + \tilde{N}_{complex})} \right|^2 = \frac{(1-n)^2 + K^2}{(1+n)^2 + K^2} \tag{2.50}$$

The relation between reflectivity and dielectric constant can easily derived from equation (2.50) by simplifying it we can get,

$$R = = \frac{1 + n^2 - 2n + K^2}{1 + n^2 + 2n + K^2} \tag{2.51}$$

The solution of the square root equation is

$$n = -\left(\frac{R+1}{R-1} \right) \pm \sqrt{\left(\frac{R+1}{R-1} \right)^2 - K^2} \tag{2.52}$$

The derivation of the refractive index of eq. (2.52) is shown in (Appendix A).

Remembering that the dielectric constant is

$$n = \sqrt{\varepsilon_{eff}} \tag{2.53}$$

If we Substitute (2.52) in (2.53), we can get

$$\sqrt{\varepsilon_{eff}} = -\left(\frac{R+1}{R-1}\right) \pm \sqrt{\left(\frac{R+1}{R-1}\right)^2 - K^2} \tag{2.54}$$

2.8 Optical conductivity

The optical conductivity is the current density response to the electric field [42] and it can be determined by the imaginary part of the dielectric constant. Complex dielectric constant is previously defined to be [41],

$$\varepsilon_{complex} = \varepsilon_1 + \frac{4\pi\sigma i}{\omega} = \varepsilon_1 + i\varepsilon_2 \tag{2.55}$$

That means,

$$\frac{4\pi\sigma i}{\omega} = i\varepsilon_2 \tag{2.56}$$

Then imaginary part of the dielectric constant is,

$$\frac{4\pi\sigma}{\omega} = \varepsilon_2 \tag{2.57}$$

$$\sigma(\omega) = \frac{\varepsilon_2 \omega}{4\pi} \tag{2.58}$$

2.9 Drude-Lorentz model

The interaction of the light with atoms of resonant frequency ω_o due to the bound electrons is modeled by displacement of the atomic dipoles as damped harmonic oscillator. The

damping appeared when the oscillating dipoles are loosing their energy by collision process in solids. This can be a reason for interaction with the phonons. The electric field of the light represents the driving force that is acting on the electrons. The following equation represents the equation of motion of the electron by ignoring the nucleus motion [34],

$$m_o \frac{dx^2}{dt^2} + m_o\gamma \frac{dx}{dt} + m_o\omega_o{}^2 x = -e\hat{E} \qquad \textbf{(2.59)}$$

Where x is the displacement of the electron from the equilibrium position, γ is the damping rate e is the electron electric charge and E is the electric field of the light wave. The first term at the left hand side represents the force, the second is the damping force and the last is the restoring force. While the right hand side is the driving force caused by the light.

Considering that the AC electric field that interacts with the electron is with an angular frequency of ω, a time dependent electric field can be written in the form,

$$\hat{E}(t) = E_o \cos(\omega t + \varphi) \qquad \textbf{(2.60)}$$

E_o is the electric field amplitude and φ is the light phase, the electric field will drive the electrons by ω. Electric field can be written as

$$\hat{E}(t) = E_o \Re e^{-(i\omega t+\varphi)} \qquad \textbf{(2.61)}$$

$\Re$ is the real part of electric field.

Also the electron displacement can be written in the form

$$x(t) = x_o \Re e^{-(i\omega t+\varphi)} \qquad \textbf{(2.62)}$$

If we Substitute eq. (2.61) and eq. (2.62) in eq. (2.59), we can get

$$-m_o\omega^2 x_o e^{-i\omega t} - im_o\gamma\omega x_o e^{-i\omega t} + m_o\omega_o{}^2 x_o e^{-i\omega t} = -eE_o e^{-i\omega t} \qquad \textbf{(2.63)}$$

So that x_o which is the electron displacement from the equilibrium position is,

$$x_o = \frac{-eE_o/m_o}{\omega_o^2 - \omega^2 - i\gamma\omega} \tag{2.64}$$

This displacement produces a time varying dipole moment of p(t), where p(t) is

$$p(t) = -ex(t) \tag{2.65}$$

Let the resonant polarization $p_{resonnat}$ to be

$$p_{resonant} = Np = -eNx \tag{2.66}$$

N is the number of polarized atoms per unit volume, sub $p(t)$ in $p_{resonant}$,

$$p_{resonant} = \frac{Ne^2}{m_o(\omega_o^2 - \omega^2 - i\gamma\omega)}\hat{E}(t) \tag{2.67}$$

This equation concludes that the response to light is small unless the frequency is closed to the natural frequency ω_o.

The complex dielectric constant can be derived by considering that the electric displacement is,

$$D = \varepsilon_o \hat{E} + P \tag{2.68}$$

The polarization split into two terms, polarization results from the driving response resonant and from non-resonant polarization, so D can be written as,

$$D = \varepsilon_o \hat{E} + P_{non-resonant} + p_{resonant} = \varepsilon_o \hat{E} + \varepsilon_o \chi \hat{E} + p_{resonant} \tag{2.69}$$

χ is the electric suscability, if we assume that the material is isotropic we can get,

$$D = \varepsilon_o \varepsilon_r \hat{E} \tag{2.70}$$

Where ε_r is the relative permittivity and $\hat{E}$ is the electric field. Substitute the equations (2.70) and (2.67) into (2.69) to get,

$$\varepsilon_r = 1 + \chi + \frac{Ne^2}{m_o \varepsilon_o (\omega_o^2 - \omega^2 - i\gamma\omega)} \tag{2.71}$$

$$\varepsilon_1 = 1 + \chi + \frac{Ne^2(\omega_o^2 - \omega^2)}{m_o \varepsilon_o ((\omega_o^2 - \omega^2)^2 + (\gamma\omega)^2)} \tag{2.72}$$

$$\varepsilon_2 = \frac{Ne^2 \gamma\omega}{m_o \varepsilon_o ((\omega_o^2 - \omega^2)^2 + (\gamma\omega)^2)} \tag{2.73}$$

The derivations of equations (2.71), (2.72) and (2.73) are illustrated in (Appendix B).

Chapter Three
Experimental details

3.1 Thin film preparation

Thin films of Yb (ytterbium), gold (Au) and manganese (Mn) and ZnPC as appear in Fig (3.1) (a) and (b) are prepared by thermal evaporation technique using VCM-600 thermal evaporator under a vacuum pressure of 10^{-5} mbar which is shown in Fig (3.2) (a) and (b). Thin films are deposited onto ultrasonically cleaned glass substrates. The glass substrates were cleaned by H_2O_2 water then it was put in the ultrasonic machine. The source materials were of high purity 99.99% metal lumps. A weight of 0.14 gram of metals was set into a tungsten boat prior for evaporation. The produced films were of 150 nm thicknesses and Fig (3.1.a) shows the glass/metals films. After that, metal films were used as substrates to evaporate 0.2 gram of ZnPC powder. ZnPC was coated onto the metal films to form Yb, Au, and Mn/ZnPC thin films interfaces following the same conditions that were applied for metals. The produced films were of 750 nm thick. The thickness of the films were measured by STM-2 thickness monitor (item-1 in Fig 3.2 (b)) that is attached to the system, the films were deposited and maintained at room temperature during the growth process.

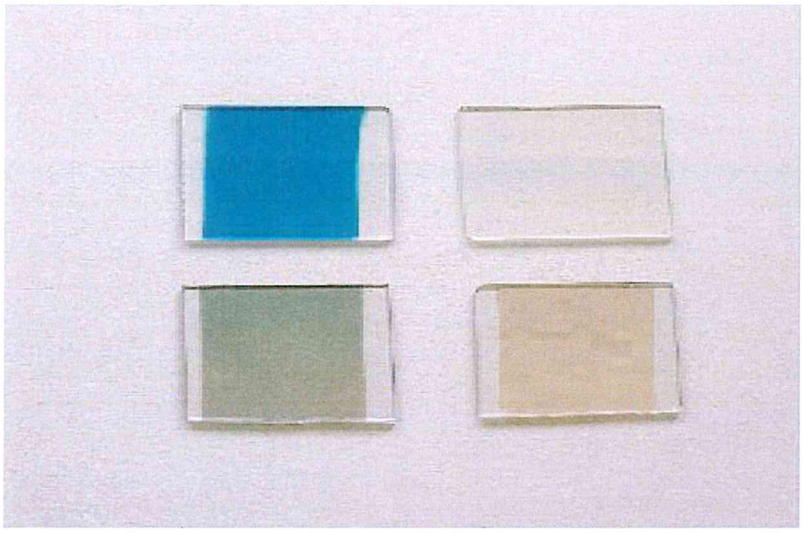

Fig (3.1.a): Thin film images of Glass/ZnPC and Glass/Yb, Au and Mn.

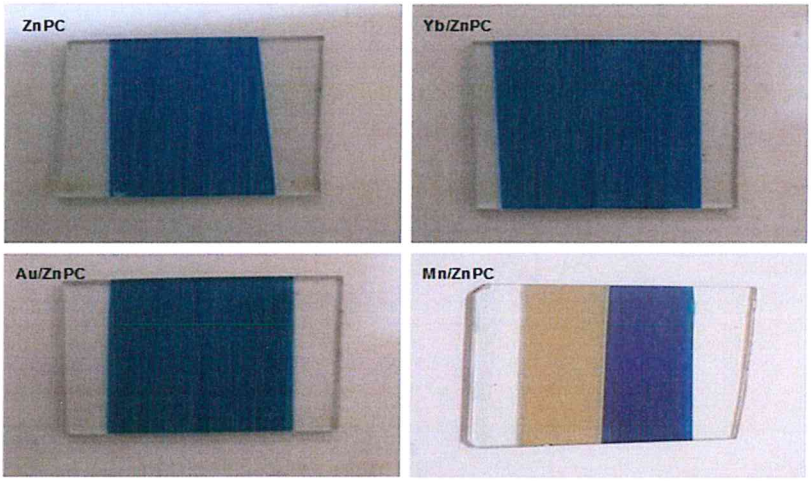

Fig (3.1.b): Thin film images of ZnPC and Yb, Au and Mn/ZnPC interfaces.

Fig (3.2): The evaporation machine.

3.2 X-ray diffraction measurements

Thin films were subjected to the X-ray diffraction technique by using Miniflex 600 X-ray diffractometer that is connected to the system. The measurements were carried out by the miniflex program with a scanning speed of 1°/min and with a diffraction angle starting from 5° up to 70°. The X-ray device is shown in Fig (3.3).

Fig (3.3): X-Ray machine.

3.3 Optical measurements

The optical properties of the films were explored by the UV-VIS-NIR thermo scientific evolution -350 spectrophotometry technique. This technique uses a xenon-lamp light, and there are two reference beams. One for regarding the reference of the sample and the other is for the sample. Transmittance and reflectance spectral measurements were recorded in the incident light range of (300-1100 nm). The data are collected by a vision software program. The data interval was 2.0 nm. The rate speed of data registry was 1200 nm/ min. In order to determine the transmittance of the light, T baseline of 100 % have to be measured. The reflectance is measured with a 0% T baseline firstly, with the help of Pike reflectometer. The UV-VIS-NIR spectrophotometer is illustrated in Fig (3.4).

Fig (3.4): UV-VIS-NIR spectrophotometer.

3.4 Hot probe technique

Hot probe technique is a method that determines whether the semiconductor is n-type or p-type [43]. There are two contacts. One of them is heated greater than the other and called hot probe. The other called cold probe. Thermal energy of the majority carrier is higher at the hot one, so the carriers tends to diffuse away from hot probe to the cold probe that left behind a positively charged, so immobile donor atoms. The donors produce a current flow towards hot probe for p-type and away for n-type. Fig (3.5) represents the hot probe technique.

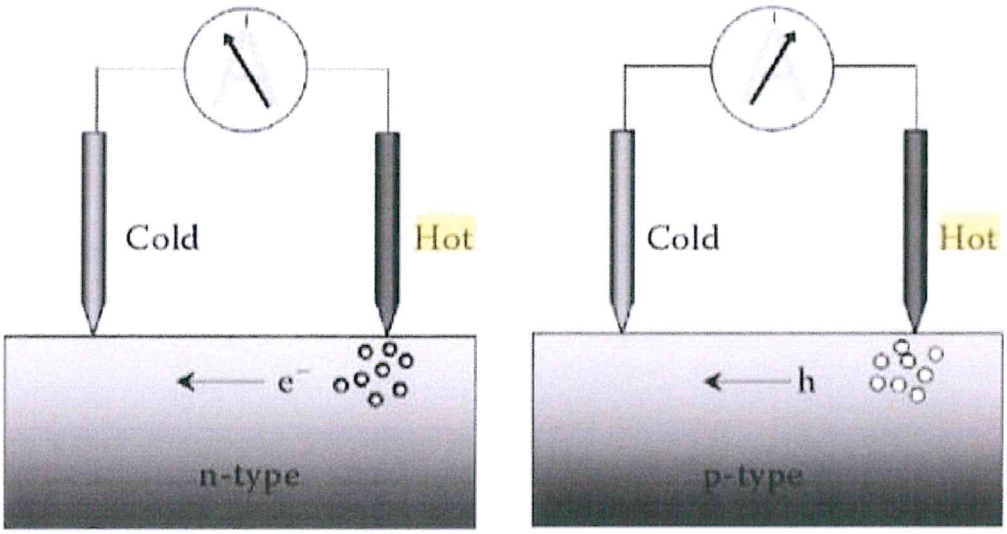

Fig (3.5): Hot probe technique.

3.5 Scanning Electron Microscope (SEM)

The scanning electron microscopy was used to produce images of the films surfaces by scanning the surface with beam of electrons. The interaction between the electrons and the atoms producing a signal that contains information about the film surface morphology. The images were taken by the SEM with enlargement of 30 K and 100K. For Yb/ZnPC films

Chapter Four
Results and Discussions

4.1 Structural properties

To explore the effects of metal substrates whose thicknesses (d) are 150 nm on the structural properties of organic zinc phthalocyanine (ZnPC) thin films (d=600 nm), the X-ray diffraction has been carried out as illustrated in Fig (4.1).

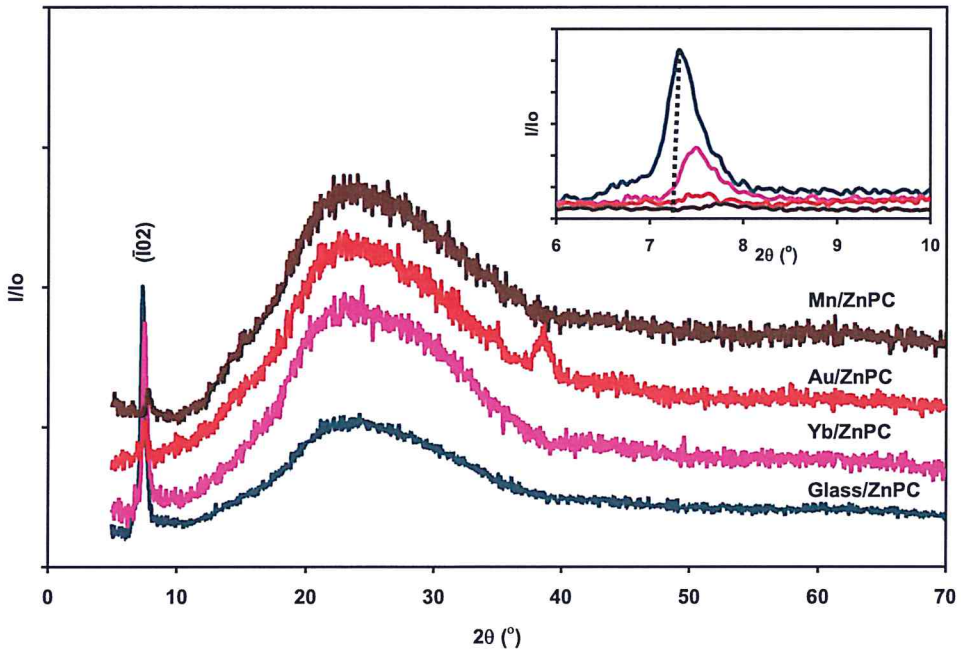

Fig (4.1): The X-ray diffraction patterns for Glass/ZnPC and Yb, Au, Mn/ZnPC interfaces.

The XRD patterns which are displayed in the figure has shown that ZnPC that was deposited onto glass substrates exhibits a crystalline nature, as at least one intensive peak appeared at $2\theta = 7.3^{\circ}$. Due to the difficulty in the analysis of just one peak, the patterns are compared with literature data. Previous investigations on ZnPC have reported that ZnPC can be either β -monoclinic or α-triclinic with lattice parameters of monoclinic cell being

a=19.3012 A°, b=4.8745 A° and c=14.5777 A° and β =120.559° [44]. The triclinic structure of α-ZnPC has lattice parameters of a= 11.668 A°, b=12.186A° and c=13.939A°, α=78.697°, β=88.045 ° and γ=62.942° [45]. The preferred orientation of the structure is determined with help of crystdiff software package that determines the lattice parameters for both monoclinic and triclinic structures. The results are shown in table (4.1). The most comparable structure to our investigations is the monoclinic, clearly β-monoclinic has an orientation of $(10\bar{2})$ at 2θ =7.20 ° which is very similar to the value we have detected in our laboratory. To obtain the error in the simulation and experimental investigations Δθ was calculated for both monoclinic and triclinic structures and they were found to be 0.10 ° and 0.33° respectively, indicating that ZnPC has a monoclinic structure oriented in $(10\bar{2})$. On the other hand, films that are deposited onto Ytterbium (Yb) substrate displayed an intensive peak localized at 2θ =7.5 °, with shift in the peak position toward higher angles (as shown in the unscaled inset of Fig.1). The intensity of the maximum peak decreased as compared to ZnPC that is deposited onto glass. On the other hand, ZnPC films coated onto manganese (Mn) substrates revealed an amorphous nature of growth. Films coated onto gold (Au) substrates displayed only a minor peak at 2θ=38.8 °.This peak is assigned to FCC gold being oriented in the (111) direction [46]. This means that metal substrates Mn and Au forces the structure of ZnPC to exhibit amorphous nature, most probably.

The interfacing of Yb with ZnPC doesn't alter the structure of ZnPC, the same peak position which appeared in the glass/ZnPC appeared when glass was replaced by Yb. This means that Yb ion doesn't take place in vacant sites of ZnPC. The possibility of merging of large Yb^{+3} ion in the vacant sites of Zn atoms can't occur. It was reported that the ionic

radius of Yb^{+3} (112 pm) [47] is larger than Zn^{+2} (74 pm) [48]. Moreover, the bond length that Yb^{+3} ion creates with N atoms (Yb-N) is 2.15 A° which is larger than that of Zn-N bond of (2.00 A°) [49, 50], indicating that ZnPC is not suitable host for Yb^{+3} ion. However, up to our knowledge there is no sufficient evidence in the literature that supports the existence of vacant sites in ZnPC, but previous investigations reported the presence of voids in ZnPC films [51], also we may think of our structural investigations as based on strain effects. ZnPC is known to have high value of strain, and the published data have indicated that the strain often originates from a vacancy site or point defect [6, 52].

Table (4.1): The simulation analysis for β-monoclinic and α-triclinic ZnPC.

Experimental		Simulation monoclinic		Simulation triclinic	
hkl	2θ (°)	hkl	2θ (°)	hkl	2θ (°)
$10\bar{2}$	7.3	$10\bar{2}$	7.20	$1\bar{1}\bar{1}$	7.63

To understand the effects of metals on the structural properties of ZnPC, Scherrer's equation for lattice parameters calculations were used. The crystallite size D, strain ∈, dislocations density δ(line/cm^2) and stacking faults SF% are calculated using equations (2.9), (2.10), (2.11) and (2.12), respectively, and listed in table (4.2). As the tabulated data shows, ZnPC deposited onto Yb substrate display a decreases in the strain and dislocation density. The crystallite size increased from 22 nm to 24 nm. This increase in the crystallite size, probably assigned to the less strain effect.

Table (4.2): The lattice parameters for Glass/ZnPC and Yb/ZnPC interfaces.

	D(nm)	ϵ x10^{-3}	δ (x10^{11} line/cm^2)	SF%
Glass/ZnPC	22	26	9.2	0.030
Yb/ZnPC	24	23	7.4	0.026

4.2 Morphological properties:

The surface morphology was investigated by scanning electron microscopy technique (SEM). For ZnPC films that was grown onto glass substrates obtaining well resolvable image was impossible. The only recordable image was for the films which were grown onto Yb substrate. The Mn and Au substrates didn't reveal any specific surface morphology due to the amorphous nature of the films. On the other hand, Fig (4.2.a) represents the surface morphology of the films coated onto Yb substrate. For an enlargement of 30K times, very tiny circular non systematically distributed grains can be observed. Further enlargement by look which is shown in Fig (4.2.b) display grains of average sizes in the range of 42 – 92 nm. The average grains size is 67 nm. The value is larger than that was detected by the X-ray diffraction technique. This difference is due to the method of measurement that may not have considered the existence of more than one crystallite (from XRD) in a grain (from SEM). In addition, the formation of strained structure may lead to an abnormal broadening in the X-ray peaks which may cause incorrect prediction of the grain size.

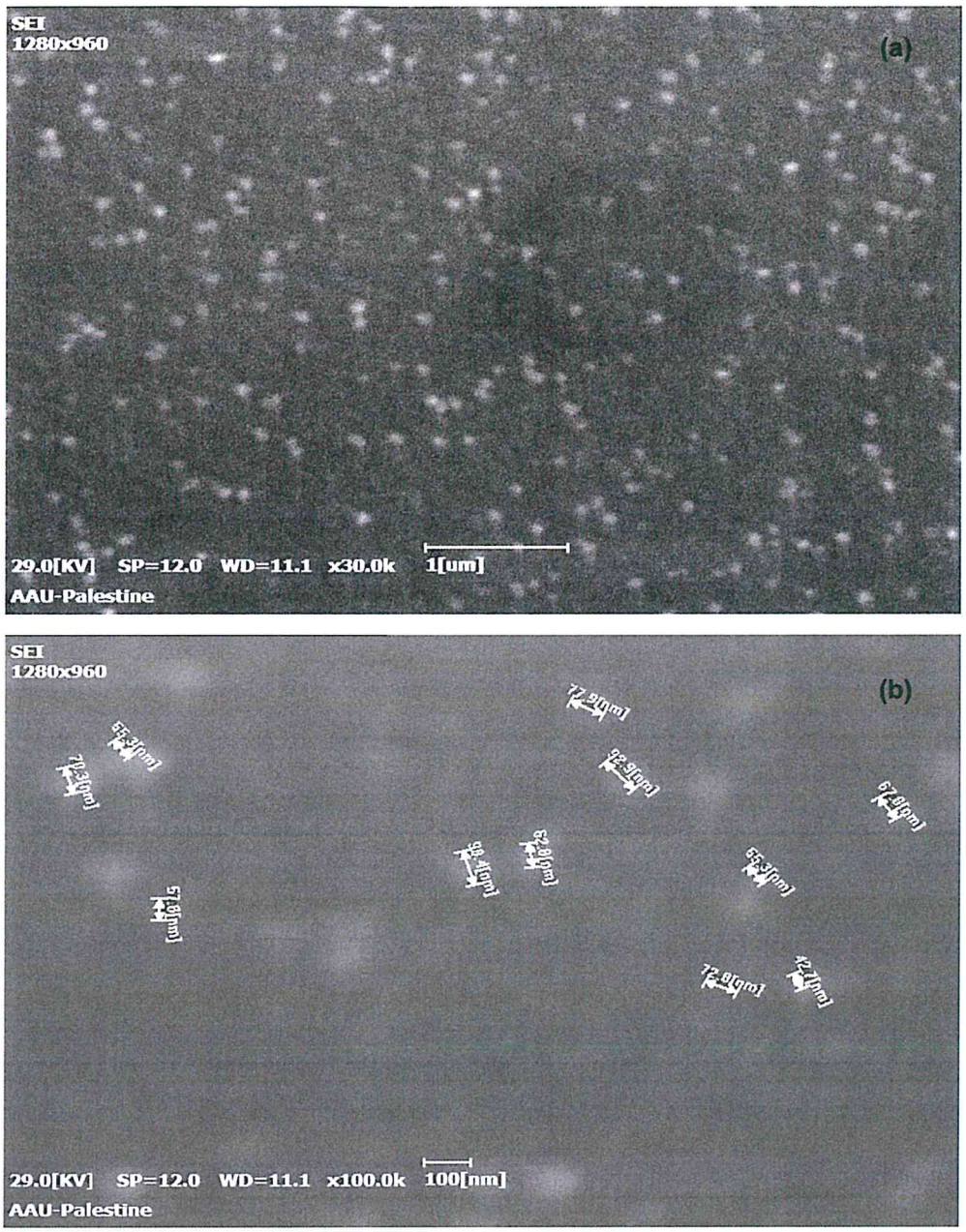

Fig (4.2): The SEM image for Yb/ZnPC interface. (a) 30 enlargement. (b) 100 enlargement.

4.3 Optical properties

To obtain deep information about the properties of ZnPC thin films, films were subjected to optical analyses. Transmittance spectra were measured in the incident wavelength of 300-1100 nm as can be seen in Fig (4.3). As the figure shows, it is noticeable that ZnPC films have two response regions to the incident light, the first response appeared in the visible light region, where the transmittance increased until reaching 450 nm then it start decreasing again. ZnPC films that are deposited onto glass substrates exhibit a maximum peak centered at 472 nm with a transmittance reaching nearly ~ 83% indicting that at this wavelength, ZnPC films become highly transparent. The coating of ZnPC onto metals decreased the transmittance percentage. Interfacing with Yb doesn't alter the peak position but lowers the transmittance. On the other hand, a shift in the peak position toward 498 nm is observed for Au/ZnPC films. Au also decreases the maxima of transmittance to 64.2 %. Moreover, two peaks are appeared for the films that are deposited onto manganese substrate. When compared to glass/ZnPC, the first peak position is shifted and the transmittance is reduced to 15.9%. The bonding mechanism and probably some vacant sites in ZnPC could have played a vital role in reducing the transmittance for Mn/ZnPC. Particularly, vacant sites of Zn may be occupied by Mn. Thus, the optical transition may take place in Mn-N bond in addition to Zn-N. Moreover, because of the smaller ionic radius of Mn^{+2} (66 pm) [53] compared with Zn^{+2} (74 pm) and the shorter bond length that Mn forms with N atoms (Mn-N) which is equal to 1.99 A^{o} [54], Mn can occupy vacant sites of Zn atoms. Other investigations confirmed that Mn can take place in ZnPC ring with four nitrogen atoms surrounding it without changing the coordination number of Zn atom [55].

In addition to the first response of ZnPC films, the second response is in the Infrared region (IR), and they followed the same sequence like that of the visible region. ZnPC has the highest transmittance in accordance with the sequence Yb, Au and Mn.

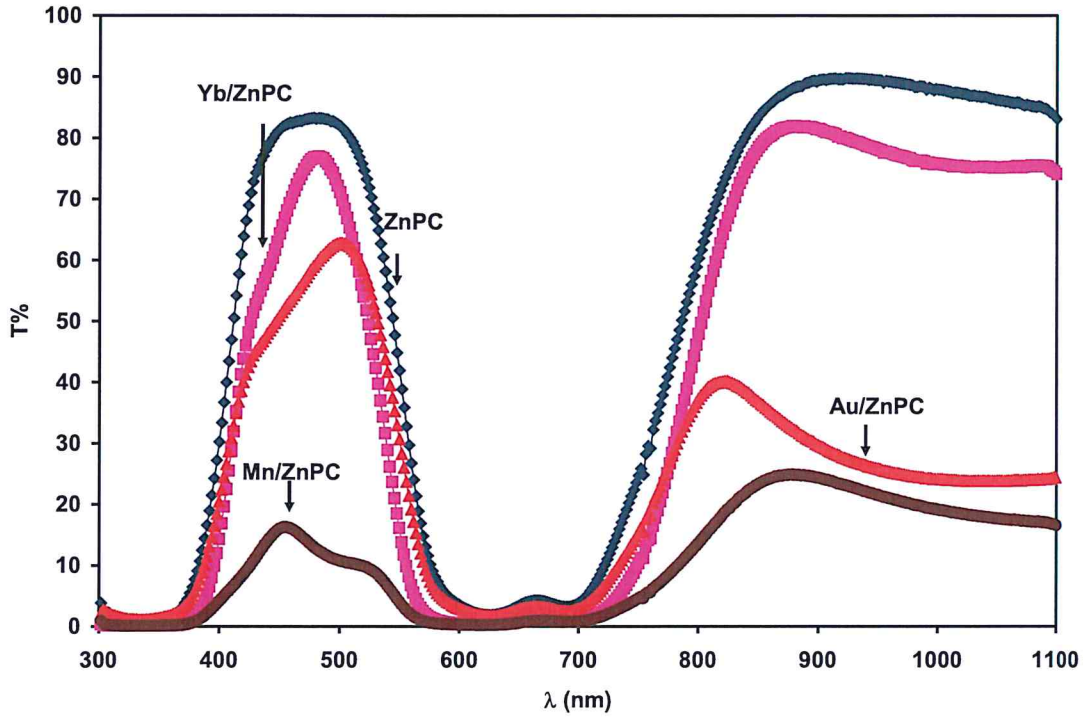

Fig (4.3): The transmittance spectra for ZnPC, Yb, Au and Mn/ZnPC interfaces.

In addition to the transmittance analysis, the reflectance spectra are recorded and presented in Fig (4.4). The studied films also exhibit response in both IR and visible region. In the visible region of light, ZnPC films displays two peaks at 472 and 892 nm, while the highest reflectivity of 19.3% is achieved for Mn films. Films of Mn, Yb/ZnPC interfaces have shown a shift in two peaks. On the contrary, Au reveals one peak in that region and the second peak disappeared. In the IR region all ZnPC films coated onto metals display

reflectivity values higher than glass/ZnPC near 1000 nm. Au has the highest reflectivity (25.7%), followed by Mn (24.3%) then Yb (11.6%).

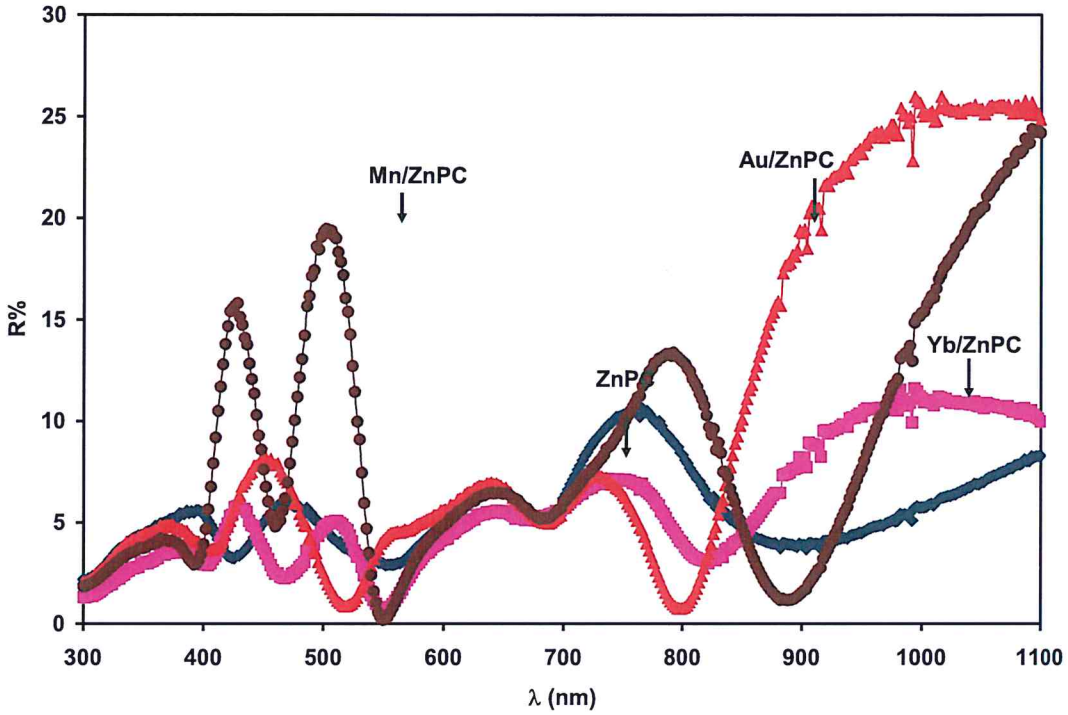

Fig (4.4): The reflectance spectra for ZnPC, Yb, Au and Mn/ZnPC interfaces.

The absorption coefficient which was calculated from the measured transmittance and reflectance according to equation (2.16) is illustrated in Fig (4.5).

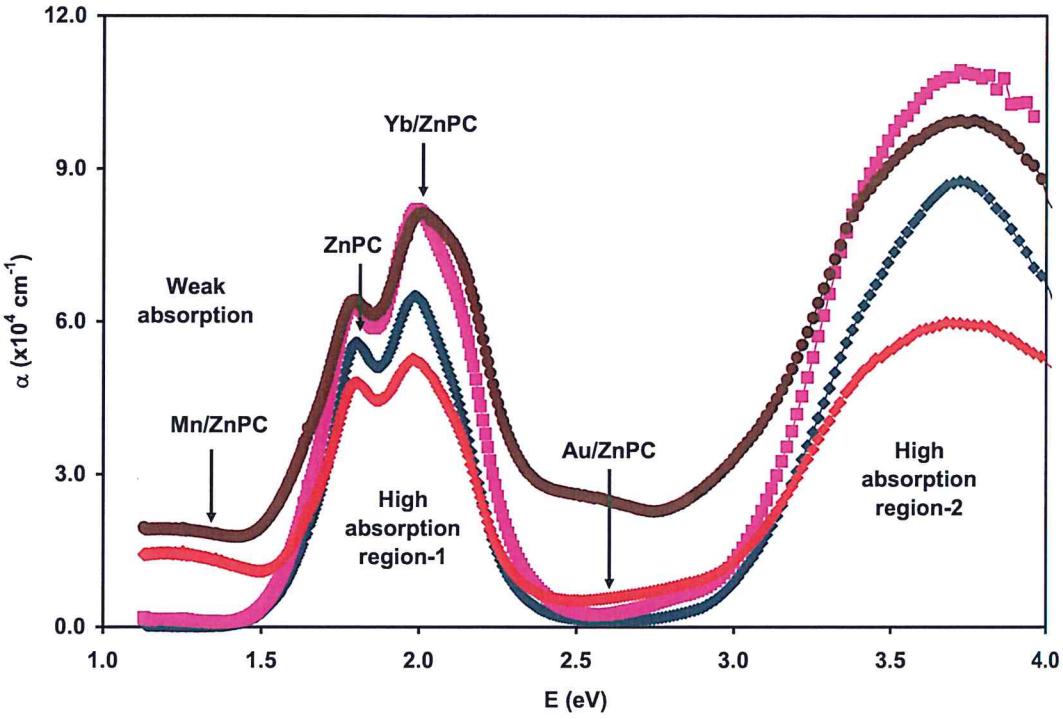

Fig (4.5): The absorption coefficient spectra for ZnPC and Yb, Mn and Au / ZnPC interfaces.

As can be seen, ZnPC films represent four absorption regions, the low absorption, moderate absorption region and two high absorption regions. The absorption coefficient response to the light clearly appeared in the high absorption regions. The moderate region didn't strongly affect the absorption coefficient except the Mn, it causes a small absorption in this region compared with ZnPC and Au, Yb/ZnPC interfaces. Weak absorption region appears in the incident photon energy of 1.1-1.5 eV, which is probably governed by the band tails. These are called "urbach energy" and determine the width of band tails (E_e) which exist in the band gap. E_e appears in amorphous and crystalline films as well [56]. The energy band tails can exist as a result of defect disorder in organic materials [56], or

inhomogeneity in the film surface [57]. To determine the band tails urbach equation (2.24) is used.

As shown in Fig (4.6), fitting of ln (α) versus incident photon energy give a straight line which allow determining E_e values.

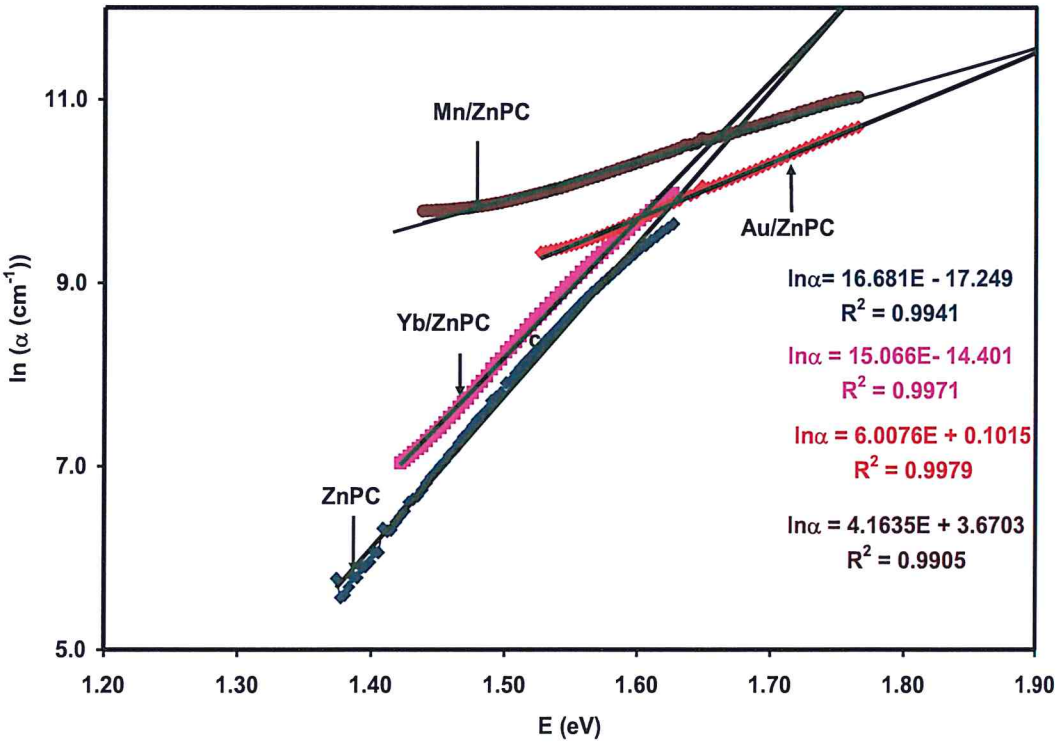

Fig (4.6): ln (α) VS photon energy spectra.

It is clear from the linearity of slopes that band tails exists in all films. The convergence point of glass/ZnPC and Yb/ZnPC interface refer to the same origin of tails, while Mn/ZnPC and Au/ZnPC interfaces refer to another tail. The band tail width for thin films,

are illustrated in table (4.3), by taking into consideration the amorphous nature of (Mn, Au)/ZnPC films, the band tail that spread among their band gaps could have arised from the random fluctuations of internal fields associated with structural disorder [58]. Moreover, Mn exhibit the largest band tails width. It was reported in other investigations that have been carried out on the transition metals that strong interaction between transition metals and semiconductors can exist with those of *3d* orbitals [59]. Now remembering that the electron configuration of Mn^{+2} is $[Ar]3d^5$, so Mn orbitals can strongly interact with ZnPC resulting in states that are localized in the band gap in addition to the already existing interbands in the pure ZnPC. The other two films coated onto Yb and Au both have *f* state that may overlap with ZnPC causing a tail states in the band gap. On the other hand, earlier studies of CdS/CdSe hetrojunctions reported interbands formation due to the vacancy of Cd in CdSe and sulfur in CdS [60]. Using this guiding information we may think that, the possibility of existence of vacant site of Zn atoms in ZnPC could also produce interbands in the band gap.

Table (4.3): Band tail width (Eα) for ZnPC, Yb, Au and Mn/ZnPC interface.

	Glass/ZnPC	Yb/ZnPC	Au/ZnPC	Mn/ZnPC
E_e(eV)	59	66	166	240

Returning back to the weak absorption region which is followed by a high absorption region (region-1). ZnPC exhibit two maxima centered at 1.80 and 1.99 eV. These peaks are

ascribed to $\pi \rightarrow \pi^*$ transitions in the Q-band absorption region. These regions represent the excitation of electron from an occupied state to a higher unoccupied state [61]. The other peak that appeared at 1.80 eV is in good agreement with that which was ascribed to the exciton states [61]. On the other hand, all metals have shown the same peak positions indicating that the optical transitions are related for ZnPC transition. Metals have induced the enhanced absorption in both of the films coated onto Yb and Mn. While Mn substrates enhanced the absorption, the Au reduces the absorption in ZnPC. The reasoning for this behavior is still unclear owing to the amorphous nature of the films. ZnPC films represent also a remarkable response of the absorption coefficient in the visible range of light (high absorption region-2) related to what is called B-band which also results from $\pi \rightarrow \pi^*$ transitions [62]. We believe that the reasons beyond this increase in the absorption in this range maybe the higher photon energy which is greater than the band gap which can create an exciton. Any further increase in the incident photon energy will saturate the absorption coefficient due to the exciton creation where no more carriers can absorb the light. Generally, organic materials display a response to the light through absorption in the form of exciton generation [51]. A previous study on ZnPC doped with lead has shown an enhancement in the absorption that is assigned to the exciton creation [63], other work that concerns with ZnPC/MoS_2 heterojunction has detected an optically excited exciton in ZnPC layer without mentioning the energy at which the exciton is detected [64].

The absorption coefficient ratios (absorbability) ($R\alpha = \frac{\alpha(Metal/\ ZnPC)}{\alpha(ZnPC)}$) were calculated and presented in Fig (4.7). Fig (4.7) shows interesting results. There is an increase in the

absorbability for Mn/ZnPC samples. It reaches maximum of ~21 times at 2.26 eV. While other films coated onto Au and Yb exhibit $R\alpha$ values of ~5 and 3~ at 2.31 and 2.38 eV, respectively. Literature data that concerns with organic ZnPC thin films reported an improvement in the efficiency of the absorbance as it is deposited onto nano-patterns polymers by ~ 14 times [65]. An improvement in the light absorbability was observed via Au/InSe interface that reached two times upon insertion InSe on Au [66]. Moreover, in another work that is interested in the absorbability enhancement of semiconductor coated onto Yb has shown that Yb increases the absorbability by 2.5 times in CdSe [67]. It seems that Yb, Mn and Au metals are more effective in enhancing the light absorbability of ZnPC than other materials.

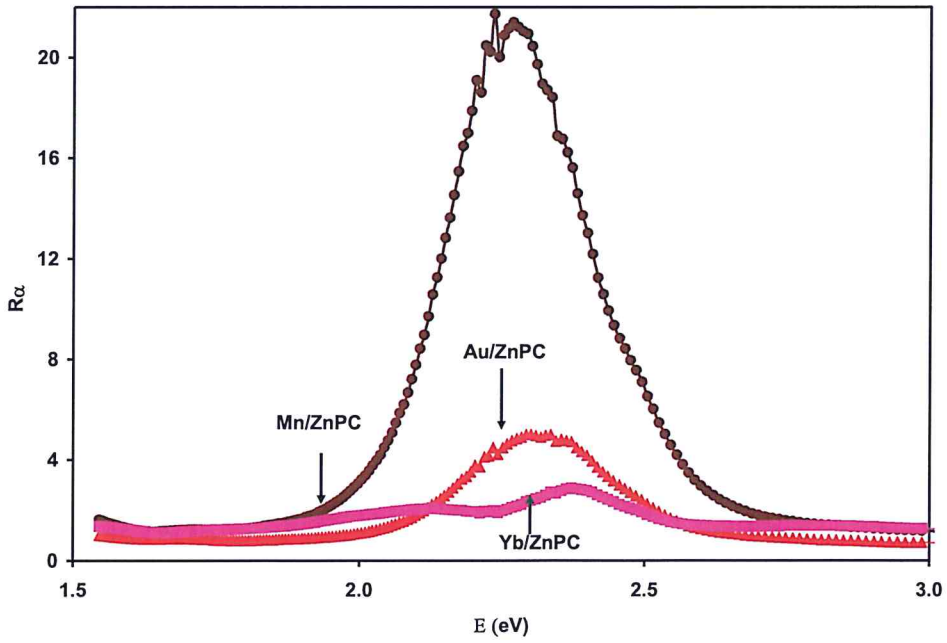

Fig (4.7): The absorbability of ZnPC and Yb, Au, Mn/ZnPC interfaces.

To explore the effect of metal substrates on the optical transitions of the films. The energy band gaps were calculated and represented in Fig (4.8), with help of Tauc's equation. The most appropriate fit is found to be for p =1/2. Fitting of $(\alpha E)^2$ versus E could be used to calculate the energy band gap where the intercept of E-axis represents the direct band gaps.

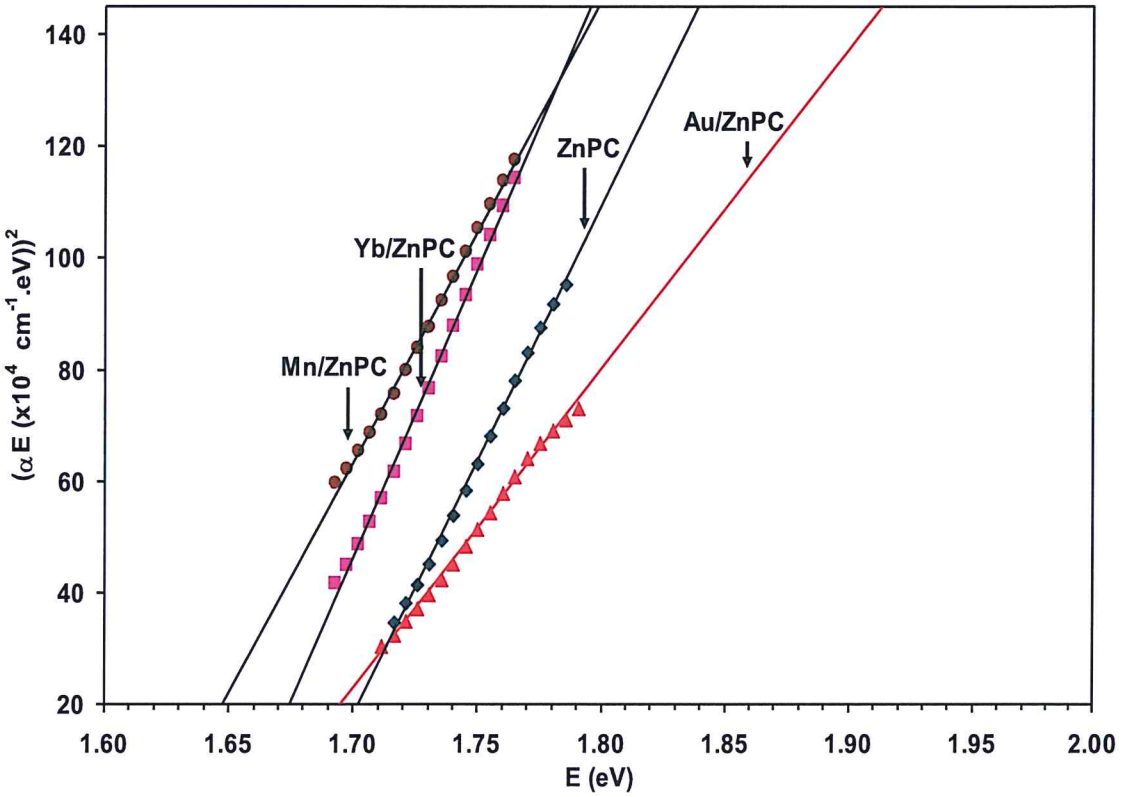

Fig (4.8): $(\alpha E)^2$ - E dependence for Q-band of ZnPC, Yb, Au, Mn/ZnPC interfaces.

The direct band gap for ZnPC is calculated for both Q and B-bands. ZnPC exhibits direct gap of 1.70 eV in the Q-band, which is very close to the literature data [68], while the metals causes a slight decrease in the band gap value. The determined band gaps are: 1.67,

1.68 and 1.65 eV for Au, Yb and Mn respectively. The energy band difference is ΔE_g = 0.03, 0.02 and 0.05 eV for Au, Yb and Mn/ZnPC interfaces respectively. In the B-band, the ZnPC films exhibit a direct band gap of 3.175 eV as appear in Fig (4.9). The metals shifted the band gap to: 3.11, 3.11 and 3.16 for Mn, Au and Yb, respectively. This slight difference in the energy band gap between ZnPC that deposited onto glass and those which deposited onto metal substrates is less significant and can be assigned to the image force lowering effects [69]. Generally, image charges builds up at the metal surface when the carriers approach the metal/semiconductor interface, an opposite charge is induced on the metal surface at the same distance, these charges are called image charges. As a result, a force of attraction is produced between the charges and induced charges that lowers the barrier energy for charge carriers.

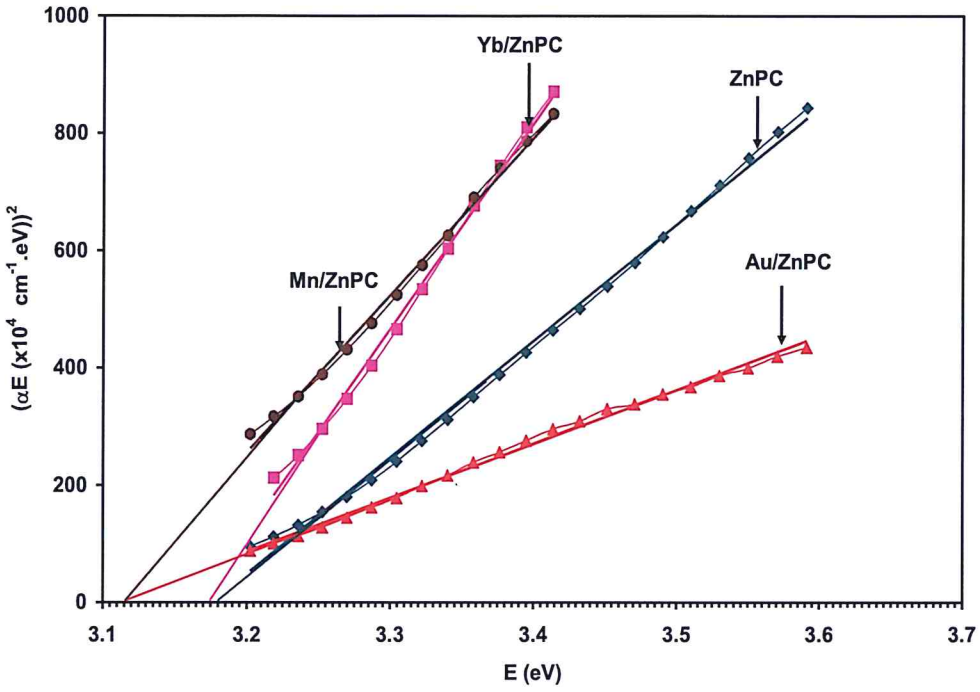

Fig

(4.9): $(\alpha E)^2$ - E dependence for B-band of ZnPC, Yb, Au, Mn/ZnPC interfaces.

4.4 Dielectric constant

The optical transmittance and reflectance data is employed to determine the dielectric spectra of the films. The effective dielectric constant can be written by equation (2.29), where the real part is determined by the equation (2.32), and the imaginary part by equation (2.33). Fig (4.10), fig (4.11) and fig (4.12) represent the real part of dielectric constant for the studied films. ZnPC films display four peaks at 1.63, 1.95, 2.63 and 3.13 eV. The peak that appeared at 1.63 eV can be attributed electronic transition from the valence to the conduction band as the band gap was determined to be 1.70 eV. While the peak which

appeared at 3.13 eV is very close to the band gap that related to B-band. Previous investigations which were carried out on H_2PC have shown an energy band gap of 2.63 eV assigned it as a fundamental energy band gap [70]. The remaining peak (1.95 eV) is also ascribed to the optical transition that is comparable to the recorded energy gap of 1.97 eV [71]. Real dielectric spectra for Yb/ZnPC and ZnPC are displayed in Fig (4.10). Yb interfacing with ZnPC altered the original patterns and caused the appearance of new peaks. The peaks appeared at 1.23, 1.66, 1.89, 2.44, 2.90 and 3.23 eV. Yb interfacing leads to highest dielectric value at 1.23 eV, the peak that is observed at 1.66 eV is nearly close to the calculated energy band gap for Yb/ZnPC interface that appeared in the Q-band. The peak which is detected at 2.90 eV is assigned to transitions between Zn-N bonds [72]. A band gap of 2.90 eV is reported for Zn_3N_2. While the peak which appeared at 2.44 eV relates to a fundamental indirect band gap of pthalocyanine (H_2PC) [73]. The peak of 3.23 eV can be assigned to the B-band transitions in Yb/ZnPC. The peak that is observed at 1.23 eV can also be ascribed to the transitions in Zn_3N_2 [74]. On the other hand, shifts in the peaks position upon semiconductor metal interfacing can be ascribed to the schottky nature of that p-type ZnPC. As the work function of ZnPC is 4.5 eV [75] when interfaced with Yb (work function of 2.5 eV) [76], it causes a schottky type band bending at the energy band interface forming the Schottky contact which is a metal semiconductor interface, when metals makes contact with semiconductor, a barrier is formed at the metal semiconductor interface.

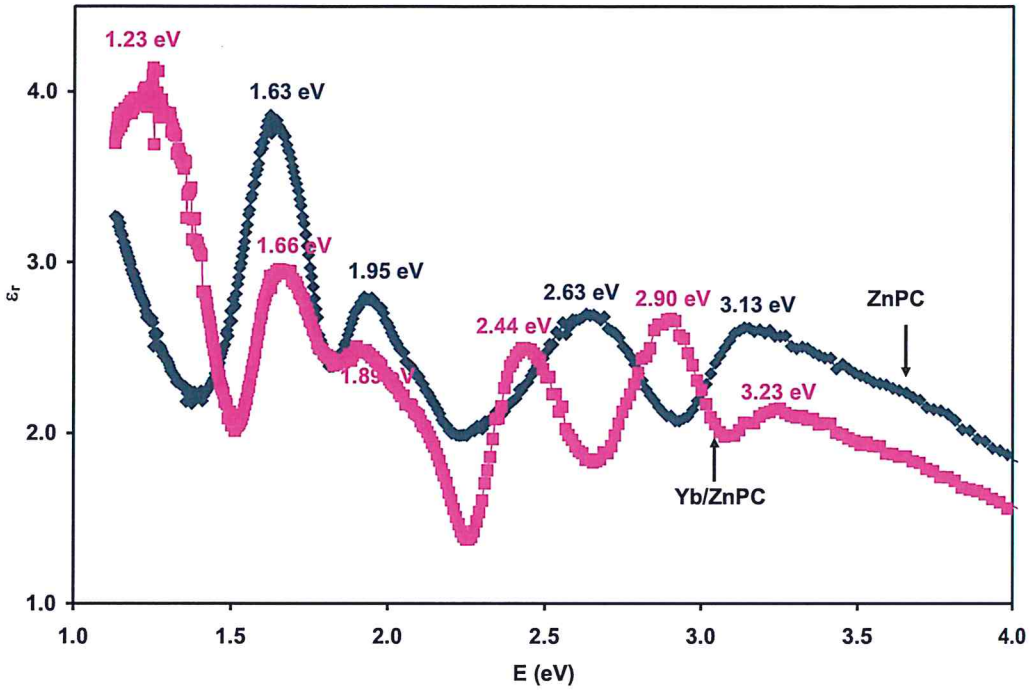

Fig (4.10): Real dielectric constant spectra for ZnPC, Yb/ZnPC interface.

The dielectric patterns for Au/ZnPC that are illustrated in Fig (4.11) represent a high dielectric constant at 1.22 eV. Au interfacing represents five peaks located at 1.22, 1.71, 1.95, 2.23 and 2.73 eV. The peak that is detected at 1.71 eV relate to the maximum peak emission of ZnPC that is corresponding to the fluorescence transition from s_1 to s_o [77]. In addition, Au/ZnPC exhibit dielectric resonance at 2.23 eV due to electronic transition in the Q-band which occur from HOMO to LOMU states [78]. Fig (4.12) display the dielectric spectra for Mn/ZnPC. Manganese has a remarkable enhancement of dielectric performance that correspond to high dielectric value compared to ZnPC. For example, Mn/ZnPC at 2.47 eV exhibit $\varepsilon_r = 6.60$. Mn/ZnPC shows five peaks located at 1.13, 1.56, 1.95, 2.47 and 2.90

eV. These peaks are shifted peaks owing to the schottky nature of contact. Mn caused a high dielectric constant value at 1.13 eV. This peak is assigned to the transitions of unpaired electron in $ZnPC^{+1}$ cation to the conduction band [79].

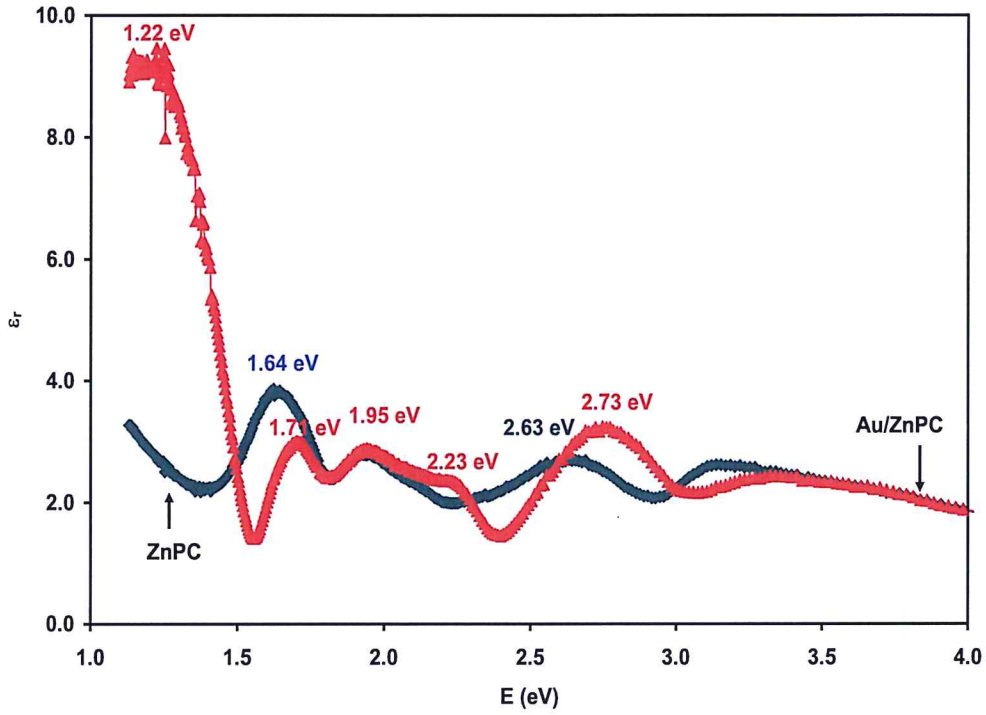

Fig (4.11): Real Dielectric constant spectra for ZnPC, Au/ZnPC interface.

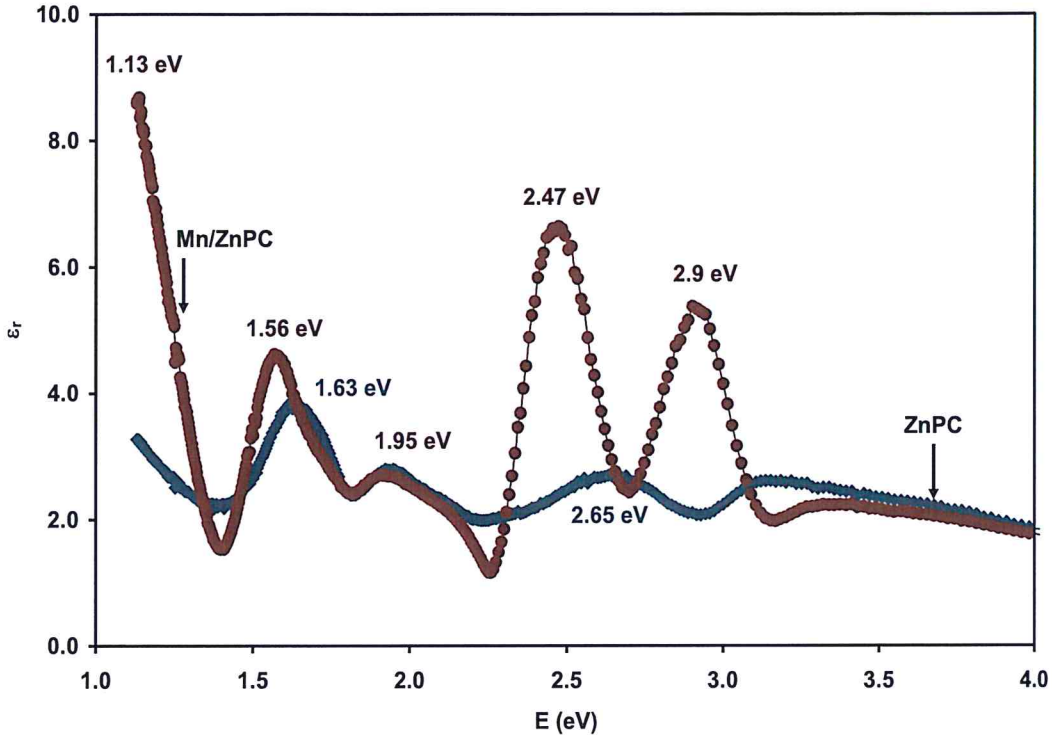

Fig (4.12): Real dielectric constant spectra for ZnPC, Mn/ZnPC interface.

The imaginary part of dielectric constant spectra is illustrated in Fig (4.13). The spectra are calculated according to the equation (2.33). ε_{im} exhibit a lower values than the ε_r. As appears from the Fig (4.13), Mn/ZnPC samples show higher values than those of Yb/ZnPC and ZnPC. Au/ZnPC displays the lowest values of ε_{im} compared to other samples. The trend of variation of ε_{im} with E of the films are similar to absorption coefficient patterns in the range of (4.0-1.5 eV). The case is different below 1.5 eV especially for Au/ZnPC and Mn/ZnPC samples.

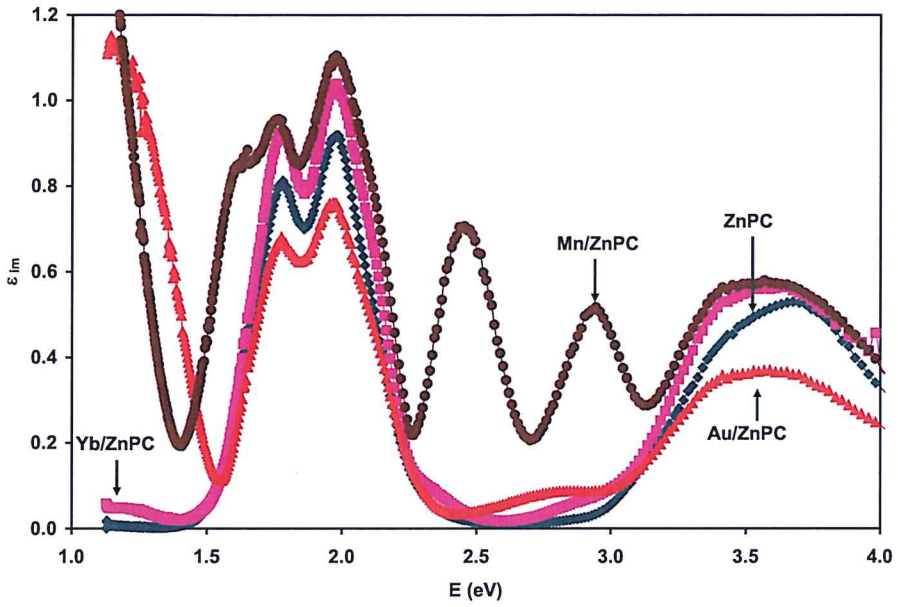

Fig (4.13): Imaginary part of dielectric constant spectra for ZnPC, (Yb, Au, Mn)/ZnPC interfaces.

Plasmon can be described as the oscillations of the electrons with respect to the positive ions in the metals. Surface Plasmons are those Plasmons that are confined to the surface and can interact strongly with light. Surface Plasmon plays a vital role in the optical properties. The modeling of ε_{im} according to Drude-Lorentz theory assuming five linear oscillators as shown in equation (2.73) display good correlation between the theoretically estimated and experimentally measured data. The theoretical estimations are shown by the green line in Fig (4.14). The computations were carried out assuming an effective mass value of $15m_o$ for ZnPC, 1.0 m_o for Yb, 1.1 m_o for Au and 1.0 m_o for Mn metals [80, 81, 82], the reduced effective mass of the double layer is determined by the equation, $\frac{1}{\mu} = \frac{1}{m^*_{ZnPC}} + \frac{1}{m^*_{metal}}$. The parameters which are obtained by the modeling

procedure are shown in table (4.4). These parameters include, electron scattering time (τ (fs)), n (free carrier density cm^{-3}), W_e (reduced frequency), W_{pe} (electron-Plasmon frequency (GHz)) and drift mobility μ (cm^2/Vs). As it can be seen, in the presence of metal substrates instead of glass, the mobility of the first oscillator (K=1), as an example, ZnPC film increased from 0.46 cm^2/Vs to 7.49, 6.86 and 7.49 cm^2/Vs when films were coated onto Yb, Au and Mn respectively. The low mobility values of ZnPC that are deposited onto glass maybe attributed to the large effective mass of holes. Also ZnPC films were reported to be an organic semiconductor with low mobility [62]. This is consistent with the value that we have got as 0.46 cm^2/Vs for the first oscillator and as 0.08 cm^2/Vs for fifth oscillator. On the other hand, we believe that the large enhancement in the mobility values of Yb and Au/ZnPC is ascribed to the large number of orbitals that Au and Yb have. From electronic point of view, the electronic configuration of both of Au and Yb are $4f^{14}\ 5d^{10}\ 6s^1$ and $4f^{14}\ 6s^2$, respectively. It was reported that the larger the orbital number and the lower the work function of metals, the larger the interaction with semiconductor and the more orbital overlapping [80]. Both of the Au and Yb exhibit large numbers of orbital but Yb have the lowest work function (2.5 eV) compared to Au (5.34 eV) [81]. For this reason Yb represent the highest overlapping leading to highest mobility. Moreover, Yb motivated the crystallization of ZnPC, in crystalline materials atoms are regularly distributed at the lattice allowing the periodic motion of electrons and the electric field distribution become uniform and the velocity of electrons increased owing to the less collisions. Previously, literature data of Yb/InSe stated that InSe exhibit mobility value of 2.53 (cm^2/Vs) compared to glass/InSe (μ= 0.2 cm^2/Vs) [83].

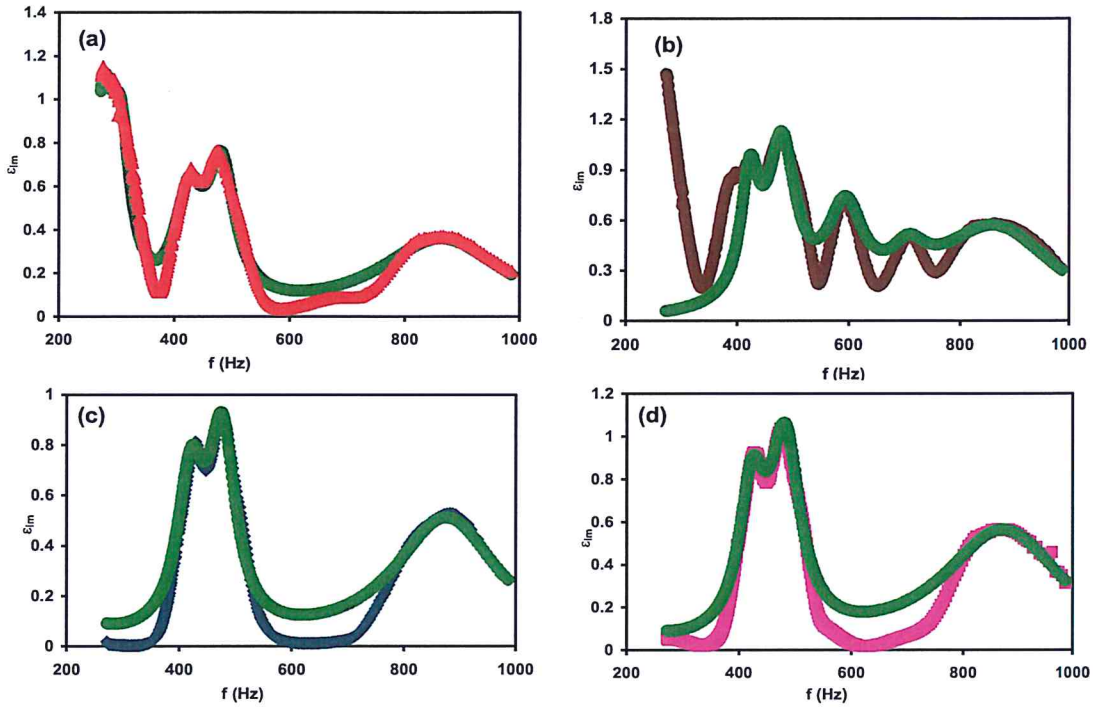

Fig (4.14): Drude-Lorentz Modeling for five oscillators for ZnPC and Yb, Au, Mn/ZnPC interfaces.

On the other hand, the free carrier density are very large for ZnPC films, in the light of these parameters modeling, we can remember that significant enhancements were achieved for Mn/ZnPC absorbability and the remarkable effect that is caused in the imaginary part of dielectric constant, can easily be understood now. The main reason maybe attributed to the large number of free carriers that absorbs the photons. The less degree of absorption in Au/ZnPC is ascribed to the smaller free carrier density. Literature data also confirmed this type of reasoning [71]. Namely, it was indicated that ZnPC films strongly absorb the visible light and create a photo generated excited carriers. In addition, the Plasmon frequency W_{pe} is regarded as an important key parameters. It indicates information about the interaction

between light and metal electrons. Since, all frequency values less than W_{pe} are reflected and those with frequency larger than W_{pe} are transmitted, the tabulated data provide information about the limitation of using ZnPC samples in optoelectronics as signal receivers.

As a complementary work, we report the optical conductivity which is calculated according to equation (2.58) and illustrated in Fig (4.15). It is noticeable that optical conductivity increases as metal substrates of Mn, Yb were used instead of glass, while Au substrate lowers it. Mn revealed the highest conductivity which is consistent with the high value of absorbability that we get. An earlier study that was carried out to discover the electrical conductivity for PC films attributed the conductivity behavior to the hole hopping through localized states during excitations [19].

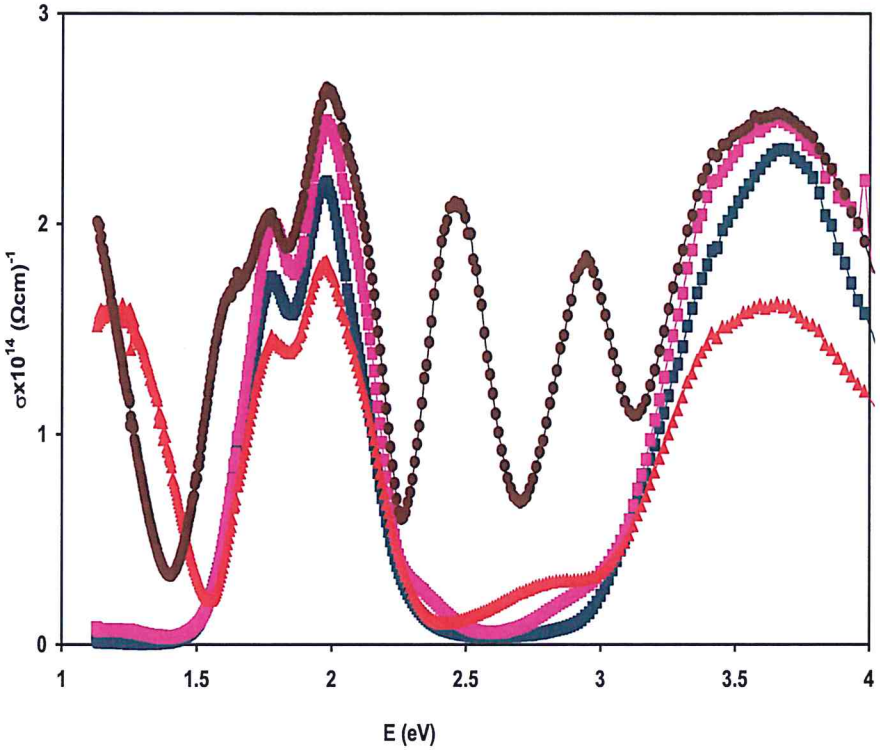

Fig (4.15): The optical conductivity of ZnPC and Yb, Au, Mn/ZnPC interface.

Table (4.4): The fitting parameters of Drude-Lorentz model ZnPC and Yb, Au, Mn/ZnPC interface.

	ZnPC					Yb-ZnPC					Au-ZnPC					Mn-ZnPC				
	1	2	3	4	5	1	2	3	4	5	1	2	3	4	5	1	2	3	4	5
τ_i(fs)	4.00	3.20	2.80	2.70	0.70	4.00	3.00	2.90	2.40	0.60	4.00	3.00	2.80	2.70	0.60	4.00	2.60	2.00	2.00	0.60
W_e ($x10^{15}$)	1.00	1.01	2.65	3.00	5.55	1.00	1.20	2.67	3.04	5.54	1.74	1.93	2.68	3.03	5.49	2.66	3.02	3.74	4.45	5.48
n ($x10^{19}$ cm^{-3})	5.00	8.00	21.0	32.0	150	0.10	0.30	1.39	2.65	12.0	0.91	0.97	1.10	1.77	8.25	1.10	2.55	2.40	1.10	11.5
μ (cm^2/Vs)	0.46	0.37	0.32	0.31	0.08	7.49	5.62	5.43	4.49	1.12	6.86	6.18	4.80	4.63	1.03	7.50	4.87	3.75	3.75	1.12
W_{pe} (GHz)	1.08	1.37	2.22	2.74	5.94	0.61	1.06	2.29	3.16	6.72	1.77	1.83	1.95	2.47	5.33	2.03	3.10	3.01	2.03	6.58

Chapter Five

Conclusions

In this thesis we reported the main structural and optical investigations on pthalocyanine (ZnPC) organic thin films. The role of metal substrate on the structural and optical performance of the films is also investigated. Various analyses using the X-ray diffraction, scanning electron microscopy and optical spectroscopy techniques has shown that the metal substrates may alter the physical characteristics of the films, significantly. Namely, while the glass and 150 nm thick Yb substrates reveal polycrystalline nature of structure, the Mn and Au substrates of the same thickness force amorphous nature of growth. In addition, the optical analyses which was carried out in the ultra violet range of light has shown that the transparent metals doesn't alter the band gap of ZnPC but created a deep interbands with width that can be engineered by the type of metal. Significant enhancement in the light absorbability at light energies of (2.2 – 2.6 eV) is achieved via using metal transparent substrates instead of glass. Moreover, the analyses of dielectric spectra arrived at the result that substrates highly increased the dielectric response in the IR region of light. Moderate response of dielectric spectra is also observed for Mn substrates. On the other hand, the modeling of the imaginary part of the dielectric spectra with the help of Drude-Lorentz approach has shown that thin metals interfacing highly enhanced the drift mobility of ZnPC to acceptable values that nominate it for use in thin films transistor technology. It was observed that while Yb substrates are suitable for forming radio wave resonator with

Plasmon frequency in the Megahertz range, the Au and Mn are more appropriate as microwaves cavities owing to the Plasmon frequency in the gigahertz range.

References

1. Schünemann, C., C. Elschner, A. A. Levin, M. Levichkova, K. Leo, and M. Riede. "Zinc phthalocyanine—Influence of substrate temperature, film thickness, and kind of substrate on the morphology." *Thin Solid Films* 519, no. 11 (2011): 3939-3945.

2. Ukei, K. "Lead phthalocyanine." *Acta Crystallographica Section B: Structural Crystallography and Crystal Chemistry* 29, no. 10 (1973): 2290-2292.

3. Ashida, Michio, Natsu Uyeda, and Eiji Suito. "Unit cell metastable-form constants of various phthalocyanines." *Bulletin of the Chemical Society of Japan* 39, no. 12 (1966): 2616-2624.

4. Uyeda, Natsu, Michio Ashida, and Eiji Suito. "Orientation overgrowth of condensed polycyclic aromatic compounds vacuum- evaporated onto cleaved face of mica." *Journal of Applied Physics* 36, no. 4 (1965): 1453-1460.

5. Marom, Noa, and Leeor Kronik. "Density functional theory of transition metal phthalocyanines, II: áelectronic structure of MnPc and FePc—symmetry and symmetry breaking." *Applied Physics A* 95, no. 1 (2009): 165-172.

6. Senthilarasu, S., R. Sathyamoorthy, S. U. B. B. A. R. A. Y. A. N. K. Lalitha, A. Subbarayan, and K. Natarajan. "Thermally evaporated ZnPc thin films—band gap dependence on thickness." *Solar energy materials and solar cells* 82, no. 1-2 (2004): 179-186.

7. Zhou, Ying, Tetsuya Taima, Tetsuhiko Miyadera, Toshihiro Yamanari, and Yuji Yoshida. "Structural modifications of zinc phthalocyanine thin films for organic photovoltaic applications." *Journal of Applied Physics* 111, no. 10 (2012): 103117.

8. Choi, Seungchel, Sang- Hyun Hong, Shin Hyo Cho, Samdae Park, Su- Moon Park, Ohyun Kim, and Moonhor Ree. "High- Performance Programmable Memory Devices Based on Hyperbranched Copper Phthalocyanine Polymer Thin Films." *Advanced Materials* 20, no. 9 (2008): 1766-1771.

9. Van Dijken, Jaron G., Michael D. Fleischauer, and Michael J. Brett. "Solvent effects on ZnPc thin films and their role in fabrication of nanostructured organic solar cells." *Organic Electronics* 12, no. 12 (2011): 2111-2119.

10. Açıkbaş, Yaser, Murat Evyapan, Tanju Ceyhan, Rifat Capan, and Özer Bekaroğlu. "Characterisation of Langmuir–Blodgett films of new multinuclear copper and zinc phthalocyanines and their sensing properties to volatile organic vapours." *Sensors and Actuators B: Chemical* 123, no. 2 (2007): 1017-1024.

11. Senthilarasu, S., S. Velumani, R. Sathyamoorthy, A. Subbarayan, J. A. Ascencio, G. Canizal, P. J. Sebastian, J. A. Chavez, and R. Perez. "Characterization of zinc phthalocyanine (ZnPc) for photovoltaic applications." *Applied Physics A* 77, no. 3-4 (2003): 383-389.

12. Kitaneh, R. ML, M. M. Abu-Samreh, S. M. Musameh, S. M. Hraibat, and A. M. Saleh. "Dielectric characterization of semiconducting ZnPc films sandwiched between Gold or Aluminum electrodes." *Applied Physics A* 114, no. 4 (2014): 1267-1275.

13. Kannan, R. Rathes, A. Mohan, P. Issac Nelson, V. Arivazhagan, B. Vidhya, and S. Rajesh. "Effect of strain in PbSe/ZnPc stacked layers prepared by thermal evaporation method." *Journal of Materials Science: Materials in Electronics* 29, no. 9 (2018): 7041-7047.

14. Dai, Jiguang, Xiaoxia Jiang, Haibo Wang, and Donghang Yan. "Organic photovoltaic cells with near infrared absorption spectrum." *Applied Physics Letters* 91, no. 25 (2007): 253503.

15. Zeng, Wenjin, Kian Soon Yong, Zhi Ming Kam, Furong Zhu, and Yuning Li. "Effect of blend layer morphology on performance of ZnPc: C 60-based photovoltaic cells." *Applied Physics Letters* 97, no. 13 (2010): 211.

16. Hamm, F. A., and Earl Van Norman. "Transformations in organic pigments." *Journal of Applied Physics* 19, no. 12 (1948): 1097-1109.

17. Senthilarasu, S., Y. B. Hahn, and Soo-Hyoung Lee. "Structural analysis of zinc phthalocyanine (ZnPc) thin films: X-ray diffraction study." *Journal of Applied Physics* 102, no. 4 (2007): 043512.

18. Senthilarasu, S., R. Sathyamoorthy, and S. K. Kulkarni. "Substrate temperature effects on structural orientations and optical properties of ZincPthalocyanine (ZnPc) thin films." *Materials Science and Engineering: B* 122, no. 2 (2005): 100-105.

19. Ahn, Hyeyoung, and Ting-Chang Chu. "Annealing-induced phase transition in zinc phthalocyanine ultrathin films." *Optical Materials Express* 6, no. 11 (2016): 3586-3593.

20. Rajesh, K. R., and C. S. Menon. "Electrical and optical properties of vacuum deposited ZnPc and CoPc thin films and application of variable range hopping model." (2005).

21. Louis, J. Sindu, D. Lehmann, M. Friedrich, and D. R. T. Zahn. "Study of dependence of molecular orientation and optical properties of zinc phthalocyanine

grown under two different pressure conditions." *Journal of applied physics* 101, no. 1 (2007): 013503.

22. Naitoh, Yasuhisa, Takuya Matsumoto, Ken-ichi Sugiura, Yoshiteru Sakata, and Tomoji Kawai. "Self-assembled stripe structure of zinc–phthalocyanine on graphite surfaces." *Surface science* 487, no. 1-3 (2001): L534-L540.

23. Borie, Bernard. "X-Ray Diffraction in Crystals, Imperfect Crystals, and Amorphous Bodies." *Journal of the American Chemical Society* 87, no. 1 (1965): 140-141.

24. Suryanarayana, Challapalli, and M. Grant Norton. *X-ray diffraction: a practical approach.* Springer Science & Business Media, 2013.

25. Drenth, Jan. *Principles of protein X-ray crystallography.* Springer Science & Business Media, 2007.

26. West, Anthony R. *Basic solid state chemistry.* John Wiley & Sons Inc, 1999.

27. Warren, Bertram Eugene. *X-ray Diffraction.* Courier Corporation, 1990.

28. Khusayfan, Najla M., S. E. Al Garni, and A. F. Qasrawi. "Design and performance of Yb/ZnS/C Schottky barriers." *Current Applied Physics* 17, no. 1 (2017): 115-119.

29. Al Garni, S. E., and A. F. Qasrawi. "Effect of Indium nano-sandwiching on the structural and optical performance of ZnSe films." *Results in physics* 7 (2017): 4168-4173.

30. Biot, Maurice A. *Mechanics of incremental deformations.* 1965.

31. Koch, Carl C., Ilya A. Ovid'Ko, Sudipta Seal, and Stan Veprek. *Structural nanocrystalline materials: fundamentals and applications.* Cambridge University Press, 2007.

32. Shetty, M. N. *Dislocations and mechanical behaviour of materials.* PHI Learning Pvt. Ltd., 2013.

33. Levy, Roland Albert, ed. *Microelectronic materials and processes.* Vol. 164. Springer Science & Business Media, 2012.

34. Fox, Mark. "Optical properties of solids." (1970).

35. Hamaguchi, Chihiro, and C. Hamaguchi. *Basic semiconductor physics.* Vol. 9. Berlin: Springer-Verlag, 2010.

36. Luque, Antonio, and Steven Hegedus, eds. *Handbook of photovoltaic science and engineering.* John Wiley & Sons, 2011.

37. Shah, Arvind Victor. *Thin-film silicon solar cells.* EPFL press, 2010.

38. Studenyak, Ihor, Mladen Kranjčec, and Mykhailo Kurik. "Urbach rule in solid state physics." *International journal of optics and applications* 4, no. 3 (2014): 96-104.

39. Cody, G. D. "Urbach edge of crystalline and amorphous silicon: a personal review." *Journal of Non-Crystalline Solids* 141 (1992): 3-15.

40. Pankove, Jacques I. *Optical processes in semiconductors.* Courier Corporation, 1975.

41. Dresselhaus, Mildred, Gene Dresselhaus, Stephen B. Cronin, and A. Gomes Souza Filho. *Solid State Properties.* Springer-Verlag Berlin Heidelberg, 2018.

42. Schrieffer, John Robert. *Handbook of high-temperature superconductivity: theory and experiment.* Edited by James S. Brooks. New York: Springer, 2007.

43. Owens, Alan. *Compound semiconductor radiation detectors.* CRC Press, 2016.

44. Schünemann, C., C. Elschner, A. A. Levin, M. Levichkova, K. Leo, and M. Riede. "Zinc phthalocyanine—Influence of substrate temperature, film thickness, and kind of substrate on the morphology." *Thin Solid Films* 519, no. 11 (2011): 3939-3945.

45. Cui, Li-Ying, Jin Yang, Qiang Fu, Bao-Zhong Zhao, Lei Tian, and Hai-Ling Yu. "Synthesis, crystal structure and characterization of a new zinc phthalocyanine complex." *Journal of molecular structure* 827, no. 1-3 (2007): 149-154.

46. Sun, Yugang, and Younan Xia. "Shape-controlled synthesis of gold and silver nanoparticles." *Science* 298, no. 5601 (2002): 2176-2179.

47. Chen, Daqin, Lei Lei, Rui Zhang, Anping Yang, Ju Xu, and Yuansheng Wang. "Intrinsic single-band upconversion emission in colloidal Yb/Er (Tm): Na 3 Zr (Hf) F 7 nanocrystals." *Chemical Communications* 48, no. 86 (2012): 10630-10632.

48. El-Sayed, A. M. "Influence of zinc content on some properties of Ni–Zn ferrites." *Ceramics International* 28, no. 4 (2002): 363-367.

49. Boncella, James M., and Richard A. Andersen. "Preparation of Yb [N (SiMe3) 2] 2 [AlMe3] 2. A complex with four ytterbium-methyl-aluminum interactions." *Organometallics* 4, no. 1 (1985): 205-206.

50. Szybowicz, M., T. Runka, M. Drozdowski, W. Bała, M. Wojdyła, A. Grodzicki, P. Piszczek, and A. Bratkowski. "Temperature study of Raman, FT-IR and photoluminescence spectra of ZnPc thin layers on Si substrate." *Journal of molecular structure* 830, no. 1-3 (2007): 14-20.

51. Zhou, Ying, Tetsuya Taima, Yosei Shibata, Tetsuhiko Miyadera, Toshihiro Yamanari, and Yuji Yoshida. "Controlled growth off ZnPc thin filmss for phootovoltaic appplications." *Physics Procedia* 14 (2011): 221-225.

52. Khusayfan, Najla M., A. F. Qasrawi, and Hazem K. Khanfar. "Impact of Yb, In, Ag and Au thin film substrates on the crystalline nature, Schottky barrier formation and microwave trapping properties of Bi2O3 films." *Materials Science in Semiconductor Processing* 64 (2017): 63-70.

53. Liu, Yongfu, Xia Zhang, Zhendong Hao, Xiaojun Wang, and Jiahua Zhang. "Tunable full-color-emitting Ca 3 Sc 2 Si 3 O 12: Ce 3+, Mn 2+ phosphor via charge compensation and energy transfer." *Chemical Communications* 47, no. 38 (2011): 10677-10679.

54. Wang, Q., Qiang Sun, Puru Jena, and Yoshi Kawazoe. "Antiferromagnetic Coupling Driven by Bond Length Contraction near the G a 1− x M n x N Film Surface." *Physical review letters* 93, no. 15 (2004): 155501.

55. Janczak, Jan, Ryszard Kubiak, Małgorzata Śledź, Horst Borrmann, and Yuri Grin. "Synthesis, structural investigations and magnetic properties of dipyridinated manganese phthalocyanine, MnPc (py) 2." *Polyhedron* 22, no. 19 (2003): 2689-2697.

56. Studenyak, Ihor, Mladen Kranjčec, and Mykhailo Kurik. "Urbach rule in solid state physics." *International journal of optics and applications* 4, no. 3 (2014): 96-104.

57. Tshomo, S., A. K. Mohsin, B. Ismail, R. Hussin, Mn Md Yusuf, WN Wan Shamsuri, K. Deraman, and S. Sholehah Hussein. "Optical properties of Diamond like Carbon films prepared by DC-PECVD." *Malaysian Journal of Fundamental and Applied Sciences* 8, no. 2 (2012).

58. Kumar, G. A., J. Thomas, N. George, N. V. Unnikrishnan, P. Radhakrishnan, V. P. N. Nampoori, and C. P. G. Vallabhan. "Physical and optical properties of phthalocyanine doped inorganic glasses." *Journal of Materials Science* 35, no. 10 (2000): 2539-2542.

59. Alharbi, S. R., and A. F. Qasrawi. "Effect of ytterbium, gold and aluminum transparent metallic substrates on the performance of the Ga2S3 thin film devices." *Current Applied Physics* 17, no. 6 (2017): 835-841.

60. AbuSaa, M., A. F. Qasrawi, and Sufyan R. Shehada. "Dielectric and Optoelectronic Properties of InSe/CdS/CdSe Heterojunctions." *Journal of Electronic Materials* 47, no. 11 (2018): 6583-6590.

61. Hamam, Khalil J., and Mohammed I. Alomari. "A study of the optical band gap of zinc phthalocyanine nanoparticles using UV–Vis spectroscopy and DFT function." *Applied Nanoscience* 7, no. 5 (2017): 261-268.

62. Rajesh, K. R., and C. S. Menon. "Electrical and optical properties of vacuum deposited ZnPc and CoPc thin films and application of variable range hopping model." (2005).

63. Aldaghfag, Shatha A. "Photovoltaic Properties of Organic Solar Cell Based on ZnPc Doped Lead Phtalocyanine." *Journal of Computational and Theoretical Nanoscience* 16, no. 5-6 (2019): 1758-1761.

64. Kafle, Tika R., Bhupal Kattel, Samuel D. Lane, Ti Wang, Hui Zhao, and Wai-Lun Chan. "Charge Transfer Exciton and Spin Flipping at Organic–Transition-Metal Dichalcogenide Interfaces." *ACS nano* 11, no. 10 (2017): 10184-10192.

65. Han, Jiyeong, Jinho Lee, and Sanggyu Yim. "Absorption enhancement of ZnPc thin films grown on nano-patterned polymer underlayer." *Applied Surface Science* 284 (2013): 315-318.

66. Qasrawi, A. F., and M. F. Taleb. "EFFECT OF Y, Au AND YAu NANOSANDWICHING ON THE STRUCTURAL, OPTICAL AND DIELECTRIC PROPERTIES OF ZnSe THIN FILMS." *Chalcogenide Letters* 16, no. 3 (2019).

67. Alharbi, S. R. "Investigation of the structural and optical properties of the CdSe/Yb/CdSe interfaces." *Materials Science in Semiconductor Processing* 76 (2018): 1-6.

68. Senthilarasu, S., R. Sathyamoorthy, and S. K. Kulkarni. "Substrate temperature effects on structural orientations and optical properties of ZincPthalocyanine (ZnPc) thin films." *Materials Science and Engineering: B* 122, no. 2 (2005): 100-105.

69. Sze, Simon M., and Kwok K. Ng. *Physics of semiconductor devices.* John wiley & sons, 2006.

70. El-Nahass, M. M., M. M. Sallam, and H. A. M. Ali. "Optical properties of thermally evaporated metal-free phthalocyanine (H 2 Pc) thin films." *International Journal of Modern Physics B* 19, no. 27 (2005): 4057-4071.

71. Senthilarasu, S., S. Velumani, R. Sathyamoorthy, A. Subbarayan, J. A. Ascencio, G. Canizal, P. J. Sebastian, J. A. Chavez, and R. Perez. "Characterization of zinc phthalocyanine (ZnPc) for photovoltaic applications." *Applied Physics A* 77, no. 3-4 (2003): 383-389.

72. Zervos, Matthew, Chrystalla Karipi, and Andreas Othonos. "Zn 3 N 2 nanowires: growth, properties and oxidation." *Nanoscale research letters* 8, no. 1 (2013): 221.

73. El-Nahass, M. M., A. M. Farid, A. A. Attia, and H. A. M. Ali. "Structural properties and UV to NIR absorption spectra of metal-free phthalocyanine (H~ 2Pc) thin films." *FIZIKA A-ZAGREB-* 15, no. 1/4 (2006): 147.

74. Ayouchi, Rachid, Catarina Casteleiro, Luis Santos, and Reinhard Schwarz. "RF- plasma assisted PLD growth of Zn3N2 thin films." *physica status solidi c* 7, no. 9 (2010): 2294-2297.

75. Hein, Corinna, Eric Mankel, Thomas Mayer, and Wolfram Jaegermann. "Engineering the electronic structure of the ZnPc/C60 heterojunction by temperature treatment." *Solar Energy Materials and Solar Cells* 94, no. 4 (2010): 662-667.

76. Skriver, Hans Lomholt, and N. M. Rosengaard. "Surface energy and work function of elemental metals." *Physical Review B* 46, no. 11 (1992): 7157.

77. Song, Weina, Chunying He, Yongli Dong, Wang Zhang, Yachen Gao, Yiqun Wu, and Zhimin Chen. "The effects of central metals on the photophysical and nonlinear optical properties of reduced graphene oxide–metal (II) phthalocyanine hybrids." *Physical Chemistry Chemical Physics* 17, no. 11 (2015): 7149-7157.

78. Hamam, Khalil J., and Mohammed I. Alomari. "A study of the optical band gap of zinc phthalocyanine nanoparticles using UV–Vis spectroscopy and DFT function." *Applied Nanoscience* 7, no. 5 (2017): 261-268.

79. He, Xiaochuan, Gangbei Zhu, Jianbing Yang, Hao Chang, Qingyu Meng, Hongwu Zhao, Xin Zhou et al. "Photogenerated intrinsic free carriers in small-molecule organic semiconductors visualized by ultrafast spectroscopy." *Scientific reports* 5 (2015): 17076.

80. Alharbi, S. R., and A. F. Qasrawi. "Effect of ytterbium, gold and aluminum transparent metallic substrates on the performance of the Ga2S3 thin film devices." *Current Applied Physics* 17, no. 6 (2017): 835-841.

81. Skriver, Hans Lomholt, and N. M. Rosengaard. "Surface energy and work function of elemental metals." *Physical Review B* 46, no. 11 (1992): 7157.

82. Yamane, Hiroyuki, and Nobuhiro Kosugi. "Substituent-induced intermolecular interaction in organic crystals revealed by precise band-dispersion measurements." *Physical review letters* 111, no. 8 (2013): 086602.

83. Alharbi, S. R., and A. F. Qasrawi. "Plasmon-electron dynamics at the Au/InSe and Y/InSe interfaces designed as dual gigahertz-terahertz filters." *Optik* 136 (2017): 524-530.

Appendix A

In order to get equation (2.52), We see that in the low frequency limit n ≈ K and n and k are both large we can rewrite equation (2.52) in the form

$$R(n^2 + K^2 + 2n) = (n^2 + K^2 - 2n) \tag{A.1}$$

$$Rn^2 + RK^2 + 2nR = n^2 + K^2 - 2n \tag{A.2}$$

$$n^2(R-1) + 2n(R+1) + K^2(R+1) = 0 \tag{A.3}$$

If eq (A.3) divided by (R-1) it becomes,

$$n^2 + 2n\left(\frac{R+1}{R-1}\right) + K^2\left(\frac{R+1}{R-1}\right) = 0 \tag{A.4}$$

The square root of this equation can be written as the following,

$$n = \frac{-2\left(\frac{R+1}{R-1}\right) \pm \sqrt{4\left(\frac{R+1}{R-1}\right)^2 - 4K^2}}{2} \tag{A.5}$$

If eq (A.5) divided by 2, it becomes

$$n = -\left(\frac{R+1}{R-1}\right) \pm \sqrt{\left(\frac{R+1}{R-1}\right)^2 - K^2} \tag{A.6}$$

Appendix B

To derive the relative permeability that appeared in eq (2.71), we substitute (2.70) and (2.67) into (2.69) to get,

$$\varepsilon_o \varepsilon_r \hat{E} = \varepsilon_o \hat{E} + \varepsilon_o \chi \hat{E} + \frac{Ne^2}{m_o(\omega_o^2 - \omega^2 - i\gamma\omega)} \hat{E} \tag{B.1}$$

If we divided the equation by ε_o and $\hat{E}$, we get,

$$\varepsilon_r = 1 + \chi + \frac{Ne^2}{m_o \varepsilon_o(\omega_o^2 - \omega^2 - i\gamma\omega)} \tag{B.2}$$

Eq. (B.2) has two parts, the real and imaginary parts, by multiplying the third term at the left hand side with $(\omega_o^2 - \omega^2 + i\gamma\omega)$,

$$\varepsilon_r = 1 + \chi + \frac{Ne^2(\omega_o^2 - \omega^2 + i\gamma\omega)}{m_o \varepsilon_o(\omega_o^2 - \omega^2 - i\gamma\omega)(\omega_o^2 - \omega^2 + i\gamma\omega)} \tag{B.3}$$

Then eq (B.3) becomes,

$$\varepsilon_r = 1 + \chi + \frac{Ne^2(\omega_o^2 - \omega^2)}{m_o \varepsilon_o(\omega_o^2 - \omega^2)^2 + (\gamma\omega)^2} + i\frac{Ne^2\gamma\omega}{m_o \varepsilon_o(\omega_o^2 - \omega^2)^2 + (\gamma\omega)^2} \tag{B.4}$$

So that

$$\varepsilon_1 = 1 + \chi + \frac{Ne^2(\omega_o^2 - \omega^2)}{m_o \varepsilon_o(\omega_o^2 - \omega^2)^2 + (\gamma\omega)^2} \tag{B.5}$$

$$\varepsilon_2 = \frac{Ne^2\gamma\omega}{m_o \varepsilon_o(\omega_o^2 - \omega^2)^2 + (\gamma\omega)^2} \tag{B.6}$$